ELSEVIER

Soil Dynamics and Earthquake Engineering 26 (2006) 435–460

SOIL DYNAMICS AND EARTHQUAKE ENGINEERING

www.elsevier.com/locate/soildyn

Analysis of nonlinear site response using the LSST downhole accelerometer array data

Chien-Ping Lee *, Yi-Ben Tsai, Kuo-Liang Wen

Institute of Geophysics, National Central University, 300, Jungda Road, Chung-Li, Taiwan, ROC

Accepted 8 October 2005

Abstract

Both linear and nonlinear behaviors of soil deposits were evaluated by strong and weak motion data observed on the surface and at depths of 6, 11, 17, 47 m at the Large Scale Seismic Test (LSST) array in Lotung, Taiwan. The soil properties measured by well logging and by the shear wave velocity profile measured by uphole and cross-hole methods are available. Both one-dimensional equivalent-linear method and nonlinear method are used for the evaluation have been used. The synthetic records at various depths are obtained by using the records at the bottom as input motion. These synthetic records are then compared with actual records at corresponding depths. Records of 13 earthquakes are used. We find that the synthetic records obtained from a linear model match well with actual records for small input motions, but the results obtained from a nonlinear model match poorly. On the other hand, the synthetic records using both the nonlinear model and equivalent-linear model are in good agreement with the observed records for large input motions. In these cases, the predicted response spectra using the linear model consistently overestimate the observed records. The threshold distinguishing the large and small input motions is 0.04 g at depth of 47 m for the LSST data. Thus, the nonlinearity started at 0.04 g and occurred unequivocally at 0.075 g. Furthermore, the dominant frequencies shift toward lower values when input motions become large. Clearly, the observed records at the LSST site manifest nonlinearity of soil response. The hysteresis loops evaluated by the nonlinear method show a permanent strain of about 0.01% in soil layers at higher ground motion input levels in this case.

Keywords: Downhole; LSST; Equivalent-linear; Nonlinear; Hysteresis loop; PGA

1. Introduction

For some time, the nonlinear ground response during large earthquakes is a controversial subject between seismologists and geotechnical engineers. Seismologists often suppose the propagating waves as a linear elastic behavior when earthquake occurs [1]. When computing synthetic waves, the site effects can be corrected by an amplification factor [2]. On the other hand, from cyclic loading test of soil samples in geotechnical laboratory, geotechnical engineers recognize that the relationship of shear stress and shear strain of soil samples are nonlinear [3]. Thus, the nonlinear response always has been concerned when earthquake engineers compute seismic waves in soil deposits. In the past, seismologists did not take seriously for nonlinear site effects because of the lack of observed records that contained nonlinear response. In recent years, the numbers of strong motion instruments are significantly increased and the qualities of seismic records are improved. Nonlinear response of soil deposits was convincingly analyzed from observed records [4–10].

The observed records contain the source, path and site effects. In order to separate the source and path effects from the records, the spectrum ratio between the soil and reference sites was often used to get amplification factor directly [11–13]. But the reference site is not easy to choose. There might still be amplification at a reference site itself [14]. By using the downhole seismic records we can avoid this problem. The distance between the downhole and surface stations is far less than the distance between the source and surface stations. Besides, the downhole records provide a true input motion. The spectrum ratio obtained from surface to downhole records can truly represent the site response [7]. Accordingly, in this study we use downhole array records to analyze the nonlinear ground response of soil deposits.

In order to examine the nonlinear response, we compute the synthetic seismograms by one-dimensional method including linear, equivalent-linear and nonlinear models,

* Corresponding author. Current Address: Institute of Earth Sciences, Academia Sinica, No. 128, Section 2, Academia Road, Nankang, Taipei 115, Taiwan, ROC. Fax: +886 2 2783 9871.

E-mail address: cplee@earth.sinica.edu.tw (C.-P. Lee).

0267-7261/$ - see front matter © 2005 Elsevier Ltd. All rights reserved.
doi:10.1016/j.soildyn.2005.10.005

using downhole array records and the soil properties at Lotung, Taiwan. The observed and synthetic records are compared to evaluate the amplification of the soil, and to find out the lower threshold of ground acceleration to induce nonlinear ground response.

2. Data for analysis

2.1. Downhole array records

The Large Scale Seismic Test (LSST) project was jointly sponsored by the Taiwan Power Company (TPC) and the Electric Power Research Institute (EPRI, USA). Two model structures were constructed at a site in Lotung in northeastern Taiwan for soil–structure interaction research. Three surface arms and two downhole arrays were installed at the site to record the ground motions on the ground surface and at different depths.

The deployment of the LSST array on the surface is illustrated in Fig. 1a. The 1/4 scale model structure was in the center and three arms extended out at about 120° azimuthal separations. There were five accelerographs in each arm. The two downhole arrays, designated as DHA and DHB, were located on the northern arm approximately 3 and 46 m from the 1/4 model with accelerometers at depths of 6, 11, 17, and 47 m, respectively, as shown in Fig. 1b.

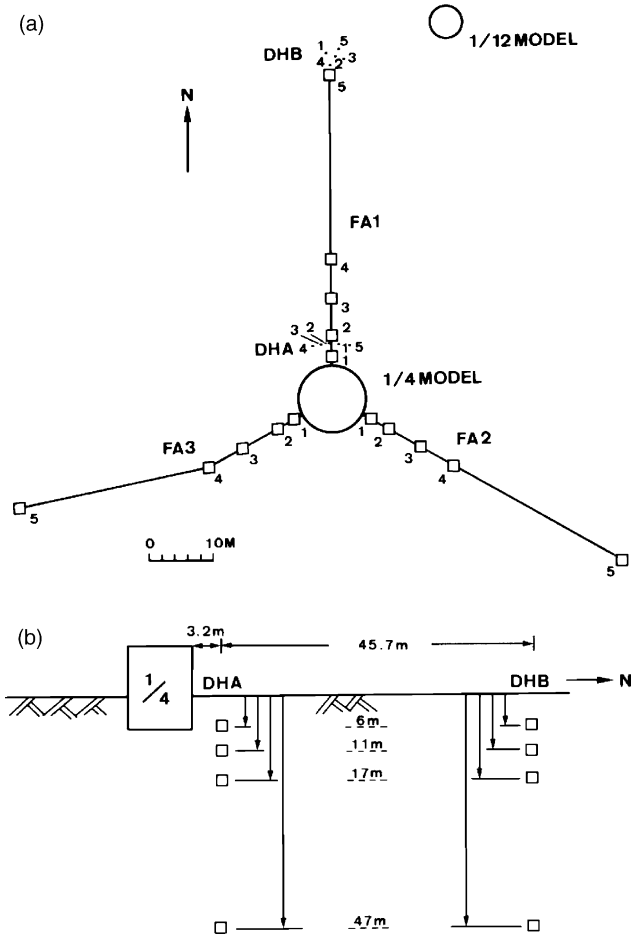

Fig. 1. (a) The layout of surface instrumentation of the LSST array. (b) The configuration of downhole instrumentation of the LSST array.

Between 1985 and 1990, a total of 30 earthquakes were recorded by the LSST array. We selected 13 of the 30 earthquakes that contained clear waveforms from most stations, and the epicentral distances were not too far. The earthquake magnitudes ranged from 3.7 to 6.2. The epicentral distances were from 4.6 to 69.2 km (see Table 1). We use the records of DHB downhole array seismometers and the fifth station of ARM-1 (FA1-5) records to study the nonlinear response of soil deposits. Because the DHB downhole array was farther away from the model structure than the DHA, its ground motions are not expected to be influenced by soil–structure interaction. The sampling rate of the records is 200 pt/s.

2.2. Soil profile

In order to simulate the response at the LSST array, we need to know the properties of local soil deposits. The well logging data was simplified to set 12 sand and three clay layers based on Chen et al. [15]. The shear modulus G_{max} at the lowest strain was determined by $G_{max}=\rho v^2$ from the shear wave velocity and the density profiles (see Table 2). In this study, we use the shear wave velocity profile measured by the uphole and cross-hole methods by HCK [16].

2.3. Shear modulus reduction curves

For one-dimensional soil response analyses, a constitutive relation that relates stress and strain is required. The normalized strain-dependent shear modulus and damping ratio of soils were determined by distortional soil sample experiments and by dynamic triaxial tests in the laboratory. In Fig. 2, the solid line represents the normalized strain-dependent shear modulus and damping ratio curves by Chang et al. [17]. And the dash line represents the mean sand curves by Seed and Idriss [18], the dotted line was the curves derived from backbone curve of hyperbolic model. Between 0.001 and 0.02% of shear strain, the shear modulus curves derived from hyperbolic model and Seed and Idriss [18] were similar with each other, but were greater than the curve by Chang for about 0.05. When shear strain was greater than 0.02%, the curves adopted by Chang et al. and Seed and Idriss were similar and the curve derives from hyperbolic model decays rapidly. We use the curves by Chang et al. and the hyperbolic model to represent the properties of local soils in this paper.

3. Analysis methods

Both one-dimensional equivalent-linear and nonlinear methods are used to calculate the site response. In the equivalent-linear method, we use the linear and equivalent-linear models for soil properties. The linear, hyperbolic, and

Table 1
The earthquake parameters and LSST array data used in this study

EQ no.	Origin time	Latitude (N)		Longitude (E)		Dist. (km)	Depth (km)	Magnitude (M)	PGA (cm/s^2)			Station no.
	y/m/d/h/m/s	Degree	Minute	Degree	Minute				V	EW	NS	
1	19851107052526	24	46.68	121	49.18	14.6	73.8	4.9	−1.9	−9.3	6.3	DHB47
2	19860116130437	24	45.77	121	57.67	23.8	10.2	6.1	22.7	−165.0	−177.9	DHB47
3	19860329071714	24	36.15	121	48.58	8.4	10.3	3.9	14.1	15.4	15.1	DHB47
4	19860408021502	24	22.72	121	47.18	31.3	10.9	4.9	4.6	−11.0	13.0	DHB47
5	19860520052600	24	4.90	121	35.48	66.1	15.8	6.2	31.4	79.4	96.9	DHB47
6	19860520053751	24	2.88	121	37.03	69.2	21.8	5.8	−5.3	14.2	−10.9	DHB47
7	19860711182525	24	37.33	121	46.95	5.0	1.1	3.7	−5.4	−28.4	16.6	DHB47
8	19860716235032	24	36.47	121	46.33	6.0	1.0	3.7	9.5	12.6	19.2	DHB47
9	19860717000333	24	39.58	121	48.90	6.1	2.0	4.3	14.6	45.6	−60.5	DHB47
10	19860730113144	24	37.72	121	47.65	5.2	1.6	5.8	90.7	143.2	186.0	DHB17
11	19860730113829	24	38.37	121	47.72	4.6	2.3	4.2	−11.1	−17.1	28.7	DHB17
12	19860805005620	24	37.05	121	46.40	5.0	1.2	4.2	14.2	56.4	58.6	DHB17
13	19871110043312	24	25.07	121	43.42	27.0	34.4	4.9	12.5	−40.9	−37.7	DHB17

empirical models are used in the nonlinear method. The methods are briefly described below.

3.1. The equivalent-linear method

The equivalent-linear method has been applied routinely in engineering community to evaluate one-dimensional soil site response using the SHAKE code [19]. This approach computes records in the frequency domain and obtains the transfer function for every layer. Consequently, the seismic wave in each layer can be obtained by convolving the input motion with the transfer function, then transforming to the time domain. We assume a trial shear modulus and damping ratio first. Then we find a new shear modulus and damping ratio corresponding with shear strain in shear modulus and damping curve using effective strain as 65% of maximum shear strain. We repeat the process until the differences of shear modulus and damping ratio are reduced below some tolerance levels.

3.2. The nonlinear method

The truly nonlinear NONLI3 code was developed by Joyner and Chen [20]. It computes in the time domain using finite difference approach, and incorporates the soil behaviors that were determined by experiments in laboratory. The nonlinear response in the soil layer was obtained in each time interval. A nonlinear explicit finite difference program DETRAN [21] which is a modified version of the NONLI3 program is used in this study to calculate nonlinear soil response.

3.3. Soil models

3.3.1. Linear model

Both equivalent-linear and nonlinear methods contain linear soil model. In the equivalent-linear method, we fix the shear modulus G_{max} at the lowest strain level. This shear modulus is associated with the shear wave velocity, and it does not change

Table 2
The soil profile model used in this study

Layer no.	Soil type	Thickness (m)	Density (g/cm^3)	Velocity (m/s)	Fs or Fc
1	Sand[a]	1.212	1.65	115.3	0.659
2	Sand	1.515	1.68	125.5	0.439
3	Clay	1.515	2.08	136.5	0.345
4	Sand	1.515	1.90	147.5	0.411
5	Sand[a]	1.515	1.81	158.6	0.396
6	Sand	1.212	1.82	166.8	0.401
7	Clay	2.424	1.97	178.7	0.527
8	Sand[a]	1.818	1.90	193.0	0.453
9	Sand	1.515	2.01	201.3	0.486
10	Clay	1.212	2.29	209.5	0.714
11	Sand	1.515	1.97	217.8	0.506
12	Sand[a]	6.06	1.97	234.3	0.627
13	Sand	6.06	1.97	244.0	0.549
14	Sand	5.912	1.97	311.5	0.485
15	Sand	12.0	1.97	261.9	0.612

Half space velocity, 2000 m/s; bottom density, 1.98 gm/cm^3; Fs, sand factor; Fc, clay factor.
[a] Means the layer with seismic sensor.

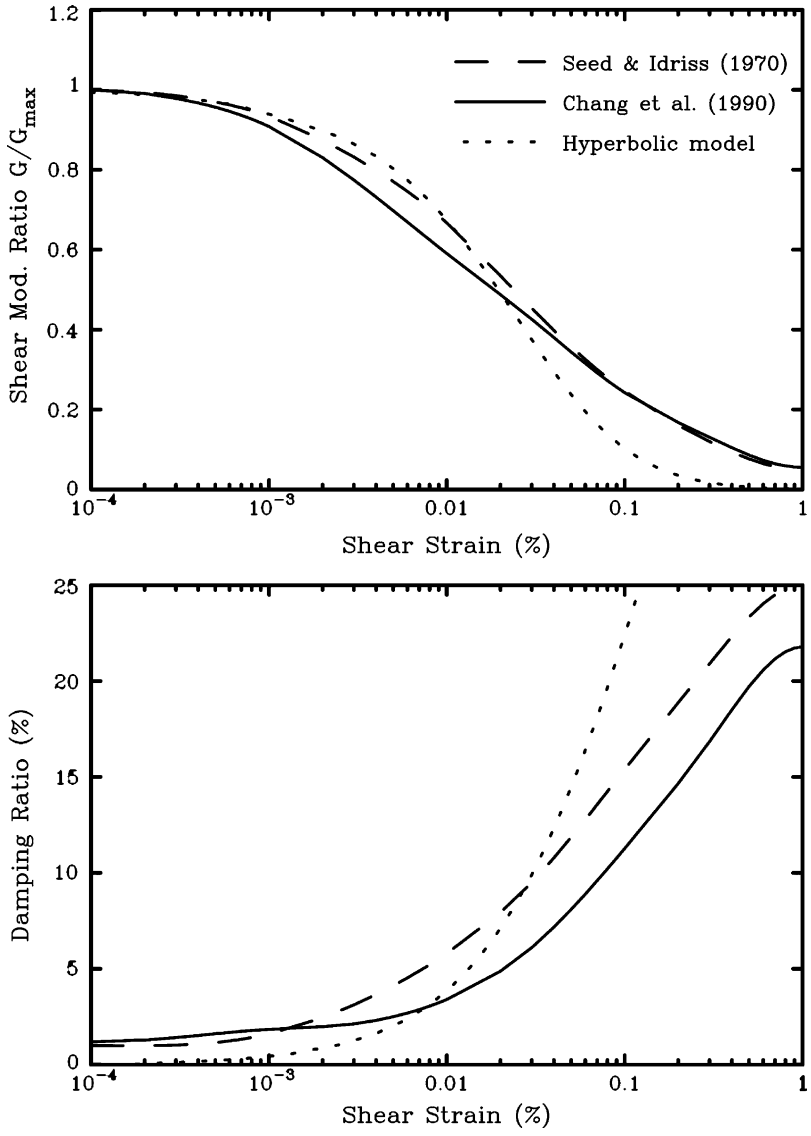

Fig. 2. The normalized strain-dependent shear modulus and damping ratio. The dash line denotes the curve by Seed and Idriss (1970). The solid line denotes the curve by Chang et al. (1990). The dotted line denotes the curve for the hyperbolic model.

with strain increase. The damping ratio is also fixed at the lowest strain level. In the nonlinear method, we set the stress–strain relation as a linear relation. Thus, its tangent line (G_{max}) passes through the origin and its slopes was 1.0 in the normalized relation. It does not change with strain increase either. In summary, we set strain-independent shear modulus and damping ratio of soil in the linear model for both the equivalent-linear and nonlinear methods.

3.3.2. Equivalent-linear model

The equivalent-linear model is not a real nonlinear model. We assume a trial shear modulus and damping first. It obtains the shear modulus corresponding with the 65% of the maximum strain, then iterates until the differences drop below a tolerance level. At last, it gives the results that approximate the nonlinear response, but its stress–strain relation is still linear.

3.3.3. Nonlinear model

When the shear modulus depends on the hysteresis loops of stress–strain relation, the nonlinear model is a truly nonlinear model. Here, we use two models in this nonlinear model. One is the hyperbolic model, and the other is the empirical model. The hyperbolic model is a theoretical model in that the initial loading curve (backbone curve) as a hyperbolic line is developed from the hysteresis loops [22]. On the other hand, the empirical model incorporates the normalized strain-dependent shear modulus and damping ratio obtained from laboratory tests to get the initial loading curve. Therefore, the stress–strain relation will develop a hysteresis loop when input motion increases. We use the normalized strain-dependent shear modulus and damping ratio obtained from Chang et al. [17] as the empirical model.

In our study, we use two models including the linear and equivalent-linear models in the equivalent-linear method and

three models including linear, hyperbolic and empirical models in the nonlinear method. At first, we find that the results obtained from linear model of these two methods are consistent with observed data for small input motions. It can explain that the linear models of the two methods are consistent in linear regime. Then we compare the difference between the equivalent-linear model of equivanlent-linear method and the nonlinear model of nonlinear method with observed data for large input motions.

4. Analysis results

Before the synthetic records are calculated, we need to process the observed data first. Because of the errors generated by baseline drift, low frequency background noise, low frequency instrumental noise, and small initial value for acceleration [23], we cannot get correct velocity and displacement waveforms directly by integrating an acceleration record. Here, a simple baseline correction and Chebyshev filter are used to correct the record. The cutoff frequencies are 0.2 and 50 Hz at low and high ends, respectively.

In this study, one-dimensional equivalent-linear method and nonlinear method have been used. The synthetic records on the surface and at depths of 6, 11, and 17 m are obtained by using the record at the bottom depth of 47 m as input motion. When there is no record available at depth of 47 m, we substitute the record at depth of 17 m as input motion to calculate the synthetic records above that depth. The depths of input motion are given in Table 1. These synthetic records are then compared with actual records at corresponding depths. One thing that needs to be cautioned is the recorded motion at depth represents a superposition of the transmitted and reflected motion from the half space. We use the recorded motion at depth as input (transmitted) motion here, thus, the input motion is an approximation in this analysis.

In total, 13 earthquakes are used in this study. The epicentral locations are shown in Fig. 3. The diamond denotes the LSST site. The source parameters are listed in Table 1. We divide these earthquakes into four groups (i.e. A, B, C, and D) according to epicentral locations and the peak ground acceleration (PGA) values in the transverse component (i.e. SH wave). Then we compare one small PGA record and one large PGA record at bottom as a pair in each group. The pair of large and small PGA records in each group ranked by ascending large PGA is designated as A, B, C, and D, respectively (see Table 3). Our purpose is to compare the site response effects at different shaking levels when the source and path effects are similar.

We use here the Group B as an example to explain the results. The Group B earthquakes include EQ6 and EQ5 which were located to the south of the LSST array at about 70 km. The magnitudes of EQ6 and EQ5 are 6.2 and 5.8, respectively. The depths of EQ6 and EQ5 are 15.8 and 21.8 km, respectively. This group is farther away from the LSST than the other three groups. The bottom input of EQ6 is at 47 m and its PGA is 0.013 g in transverse component. The bottom input of EQ5 is also at 47 m and its PGA is 0.075 g in transverse component.

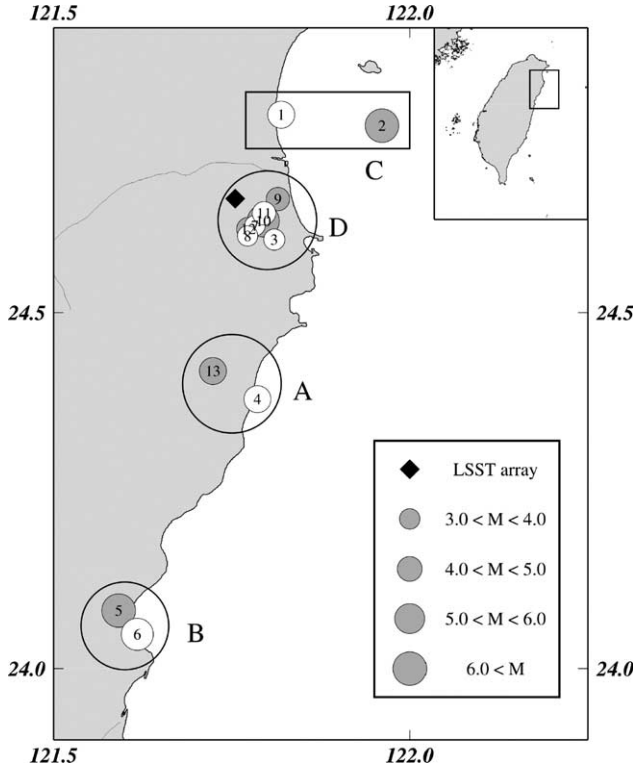

Fig. 3. Epicenters of the 13 earthquakes whose data are analyzed in this study. A, B, C, and D shows the four groups defined according to the earthquake location. The white and gray circles denote the epicenters of weak input motion and strong input motion, respectively. The diamond denotes the LSST array site.

At first, we compare the difference between the calculated records by the equivalent-linear and nonlinear method from EQ6. The results obtained from the linear model by the equivalent-linear method are shown in Fig. 4a. The accelerograms and their 5%-damping response spectrums are shown in the left hand side and right hand side of Fig. 4a, respectively. The reason we use the response spectrum instead of the Fourier spectrum is that the Fourier spectrum often needs to be smoothed by trial-and-error smoothing processes. On the other hand, the response spectrum provides a convenient yet well-defined method to demonstrate the results. The comparisons are for points on the surface, at the depths of 6, 11, 17 and 47 m from top to bottom, respectively. At each depth, the upper time history is the calculated result and the lower time history is the observed record. The thick line in the right side of Fig. 4a represents the observed record and thin line represents the calculated result

Table 3
The small and large PGA pairs in the four groups, A, B, C, and D

Group	Small PGA group	Large PGA group
A	EQ4 (PGA = 0.012 g)	EQ13 (PGA = 0.039 g)
B	EQ6 (PGA = 0.013 g)	EQ5 (PGA = 0.075 g)
C	EQ1 (PGA = 0.008 g)	EQ2 (PGA = 0.153 g)
D	EQ11 (PGA = 0.029 g)	EQ10 (PGA = 0.228 g)

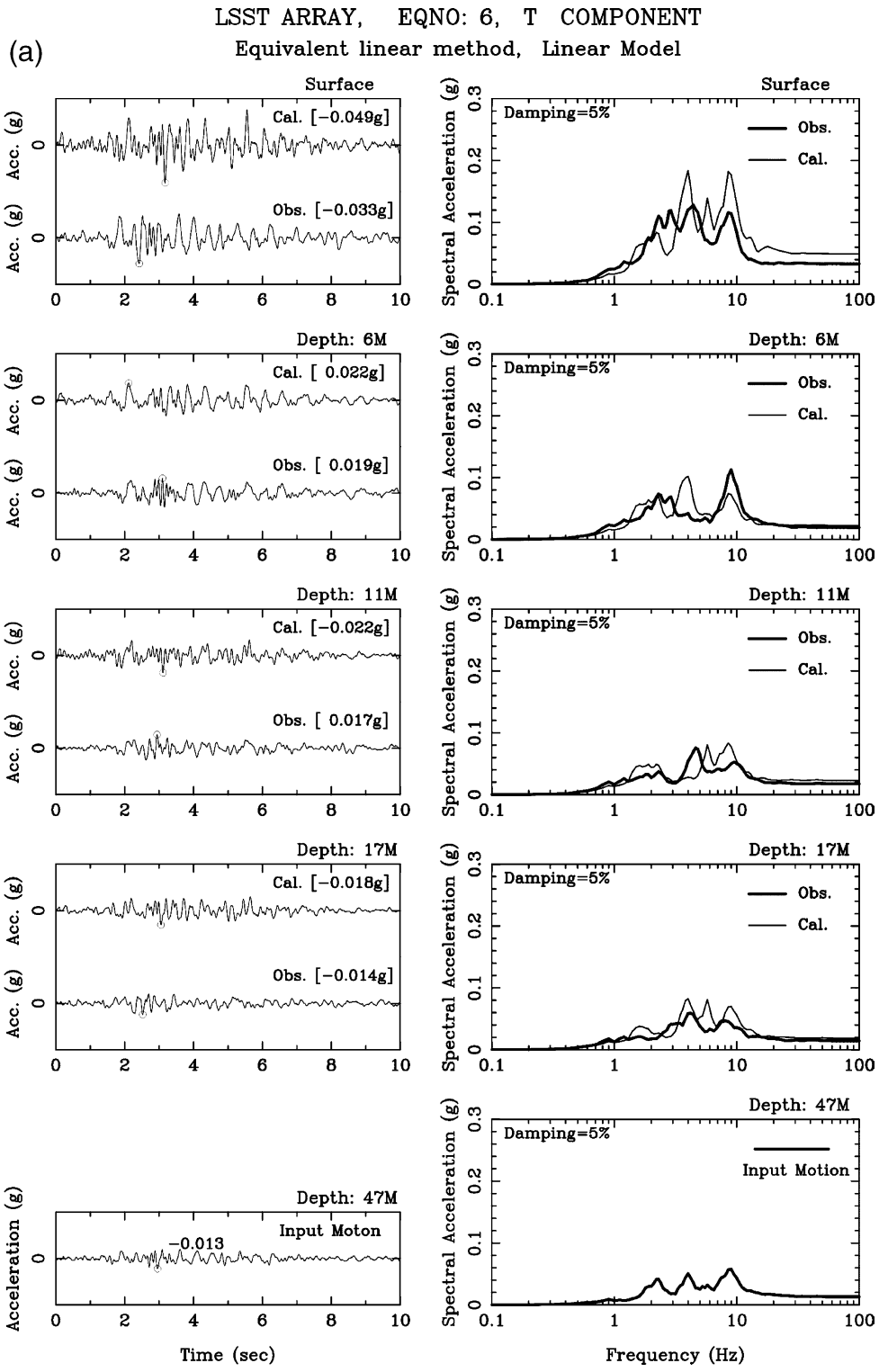

Fig. 4. (a) The results computed by EQ6 using the linear model in the equivalent-linear method. The left hand side plot shows the observed and synthetic seismograms at different depths. The right hand side plot shows the corresponding 5%-damping response spectra. (b) The results computed by EQ6 using the equivalent-linear model in the equivalent-linear method. (c) The results computed by EQ6 using the hyperbolic model in the nonlinear method. (d) The results computed by EQ6 using the empirical model in the nonlinear method.

in response spectra. This figure shows that the calculated results at different depths are quite similar with the corresponding observed records. Their spectra also are consistent with each other in the frequency domain.

Fig. 4b shows the results obtained from an equivalent-linear model by the equivalent-linear method. These results are similar to above results from the linear model. Since the records obtained from the linear soil models by the equivalent-linear and

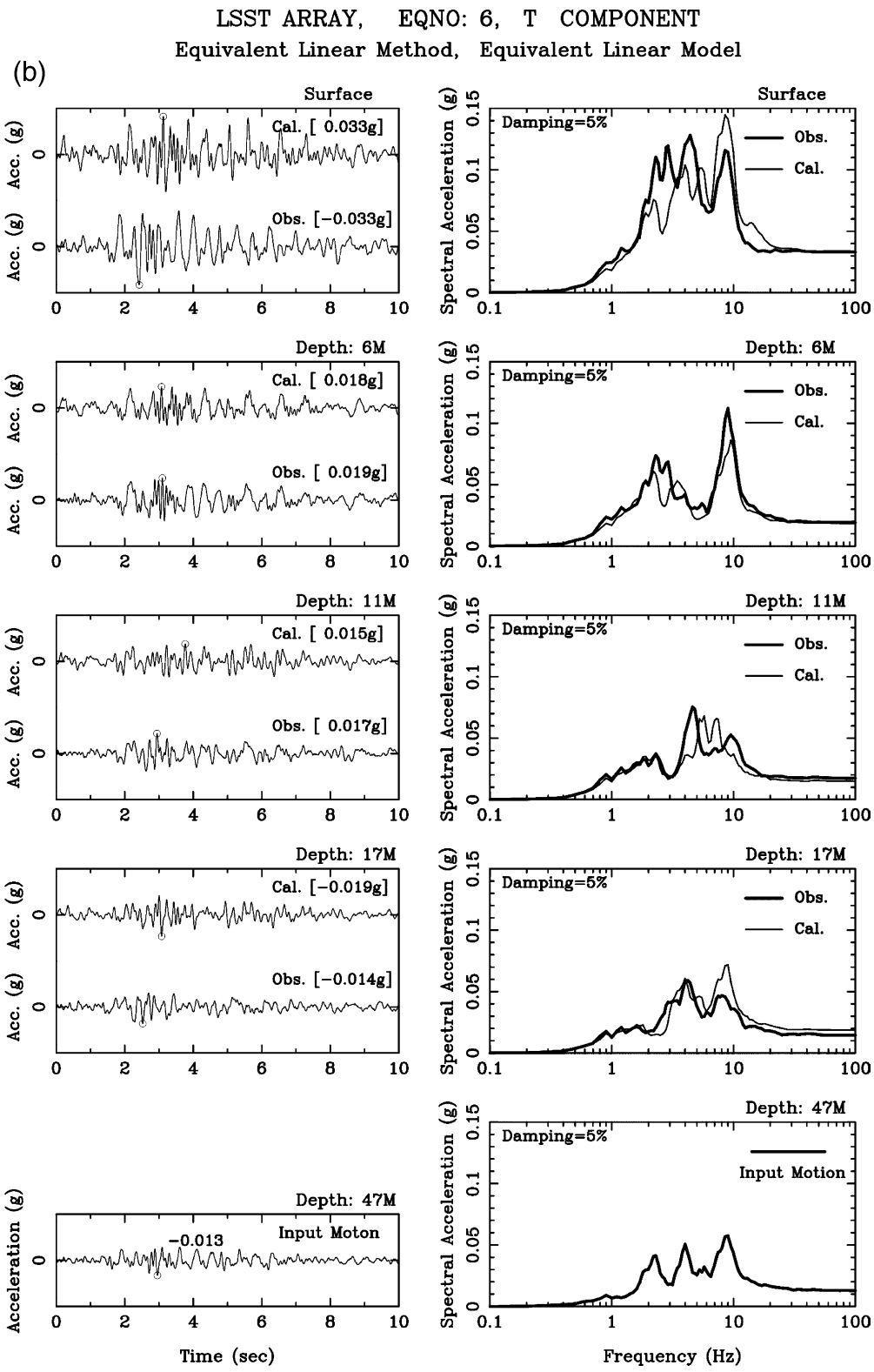

Fig. 4 (*continued*)

nonlinear methods are similar, we will only use a linear model in the equivalent-linear method to present the results below.

Fig. 4c and d show the results from hyperbolic and empirical model by the nonlinear method, respectively. The results from hyperbolic model tend to slightly underestimate in the high frequency range, and the results from empirical model obviously underestimate above 2 Hz in response spectra.

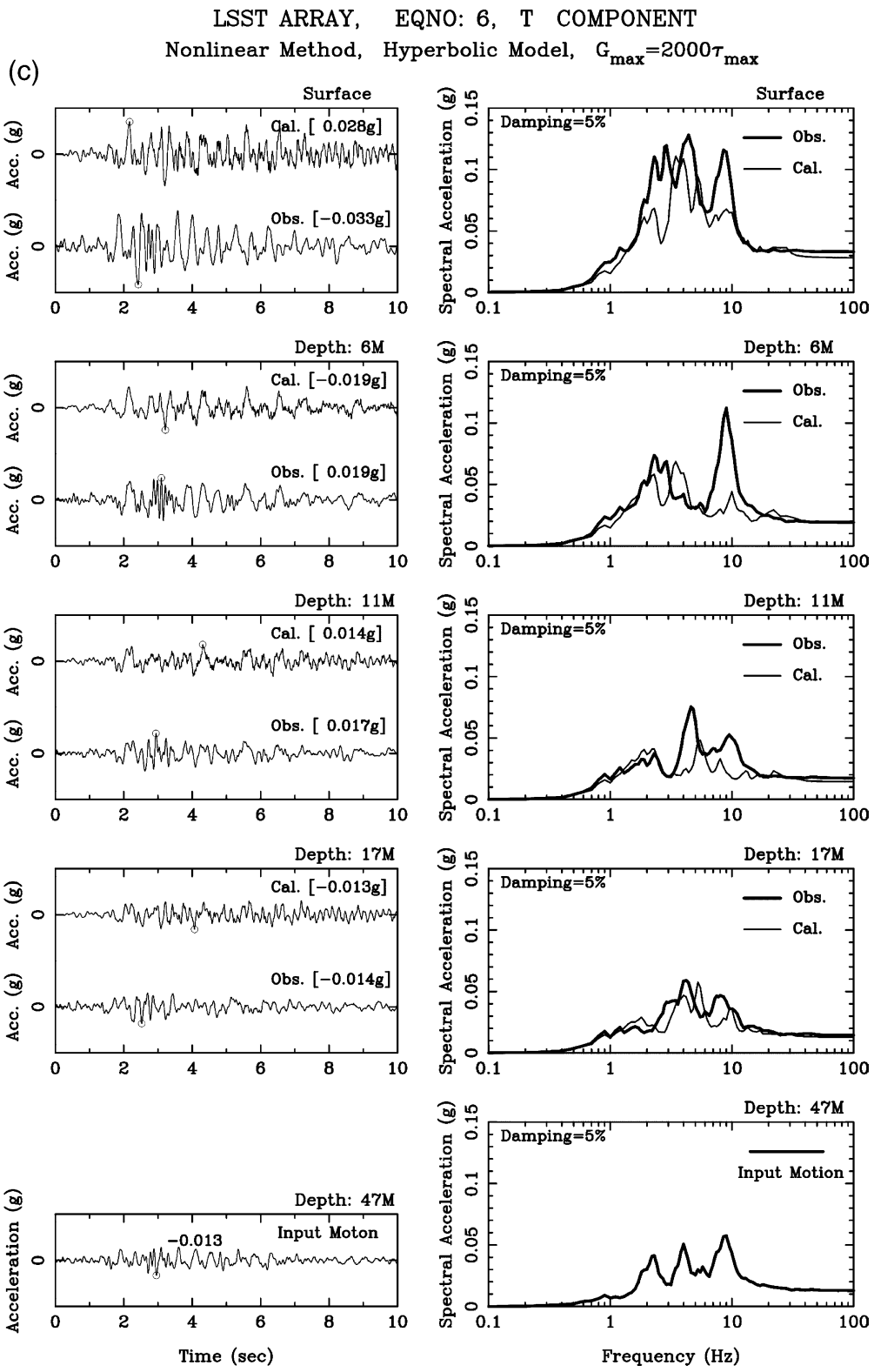

Fig. 4 (*continued*)

The input PGA of EQ5 is larger than that of EQ6 by about six times. Fig. 5a shows the results from a linear model by the equivalent-linear method. The calculated records are significantly larger than the observed records both in time histories and as well as in response spectra. On the contrary, the results from the equivalent-linear model and the observed records are in excellent agreement (Fig. 5b). The results from hyperbolic and empirical models

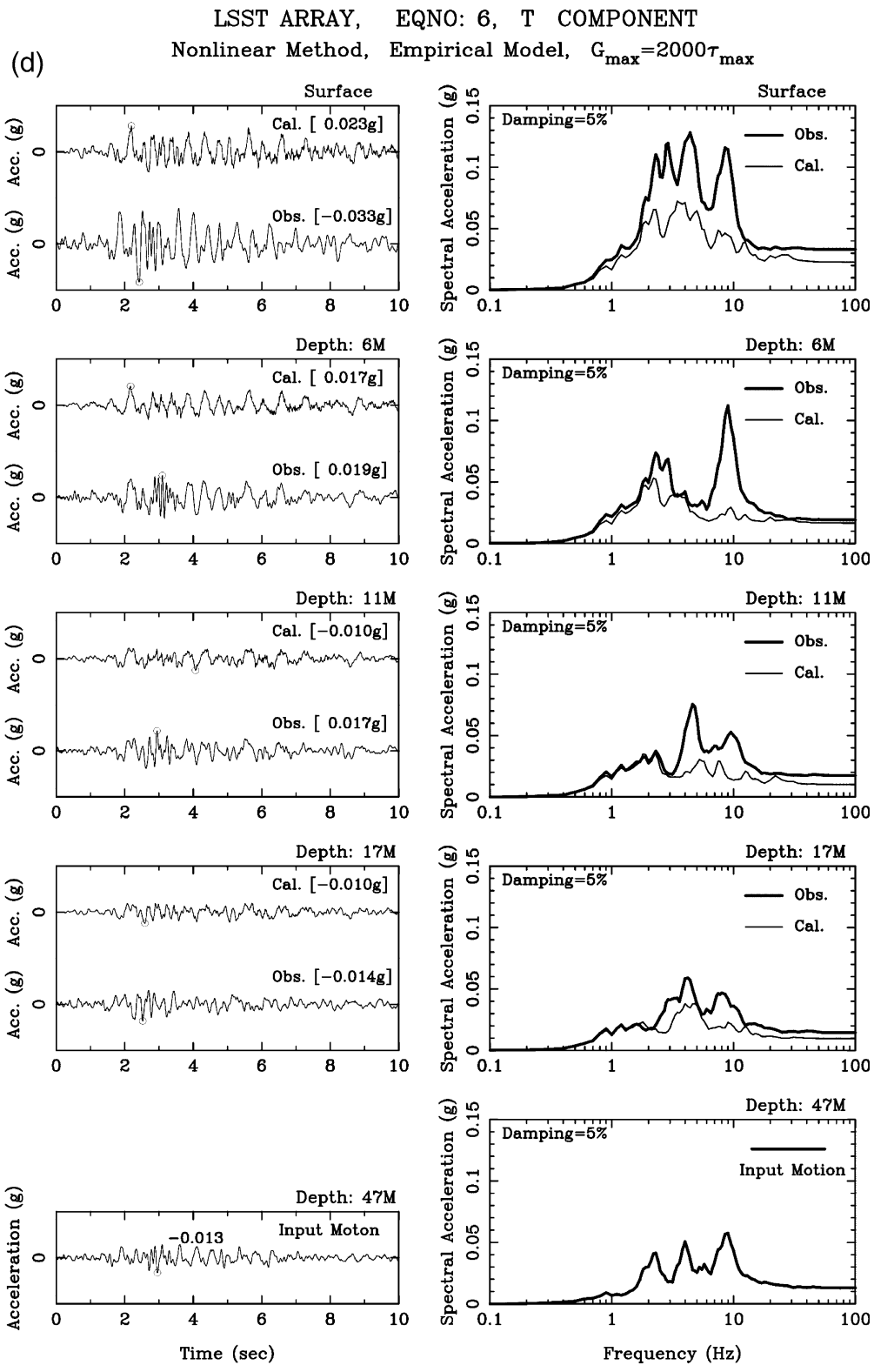

Fig. 4 (*continued*)

by the nonlinear method are also consistent with the observations (Fig. 5c and d).

Other three pairs also show similar results. From the overall results of the four pairs, we find that the calculated records obtained from both the linear and equivalent-linear model are consistent with the observed records at low level of shaking. However, the results obtained from the hyperbolic and empirical model by the nonlinear method are underestimated.

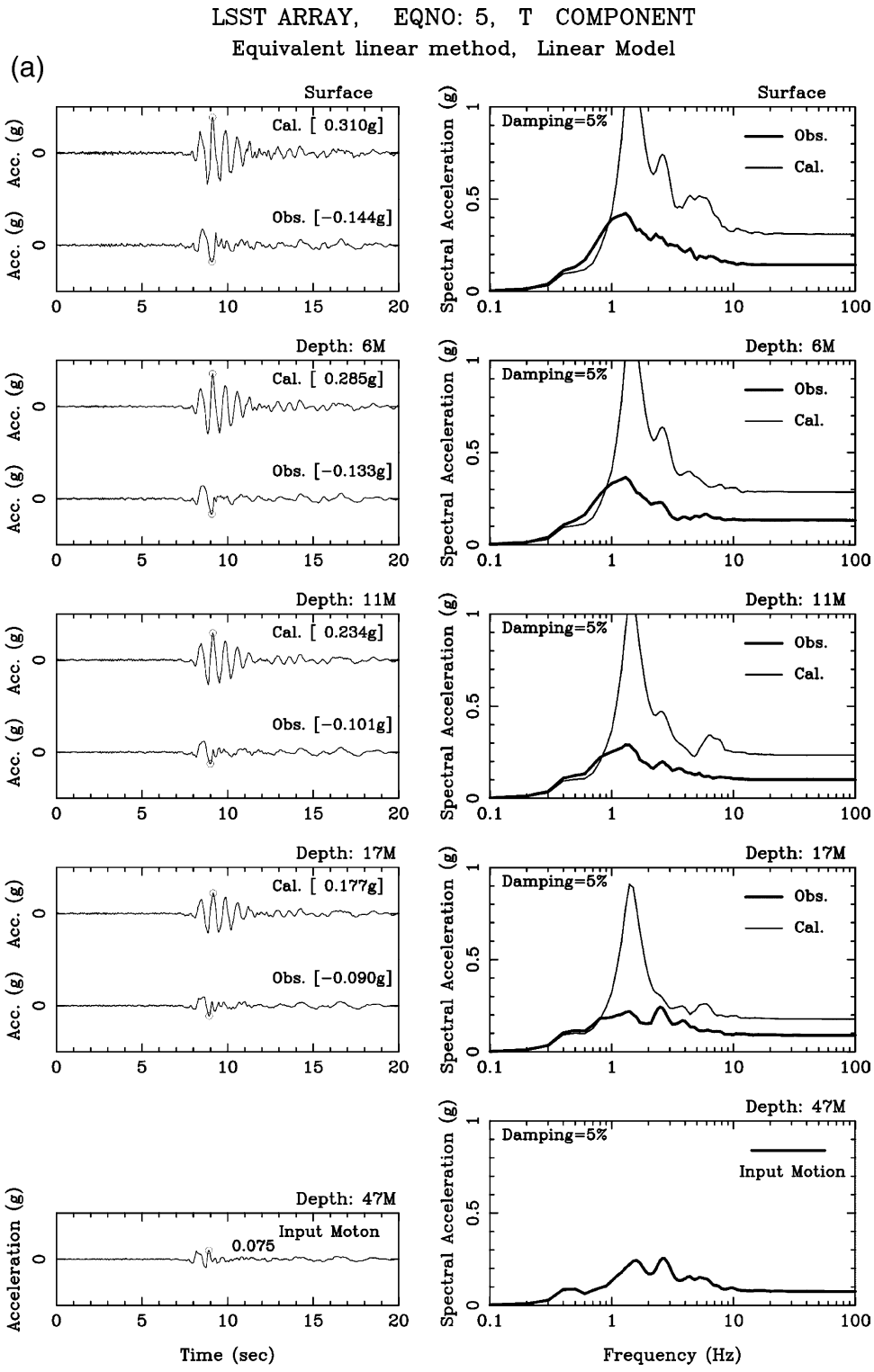

Fig. 5. (a) The results computed by EQ5 using the linear model in the equivalent-linear method. (b) The results computed by EQ5 using the equivalent-linear model in the equivalent-linear method. (c) The results computed by EQ5 using the hyperbolic model in the nonlinear method. (d) The results computed by EQ5 using the empirical model in the nonlinear method.

For large input motion, the calculated records obtained from the linear model are much larger than the observed records and are overestimating the response spectra. On the contrary, the results obtained from the equivalent-linear, hyperbolic and empirical models match well with the observed records.

The results obtained from linear model are affected sensitively by the input motion level. We divide the 13 earthquakes into two groups according to the shaking level of input motions. Seven of the 13 earthquakes with input motions smaller than 0.04 g are classified as weak events. The other six

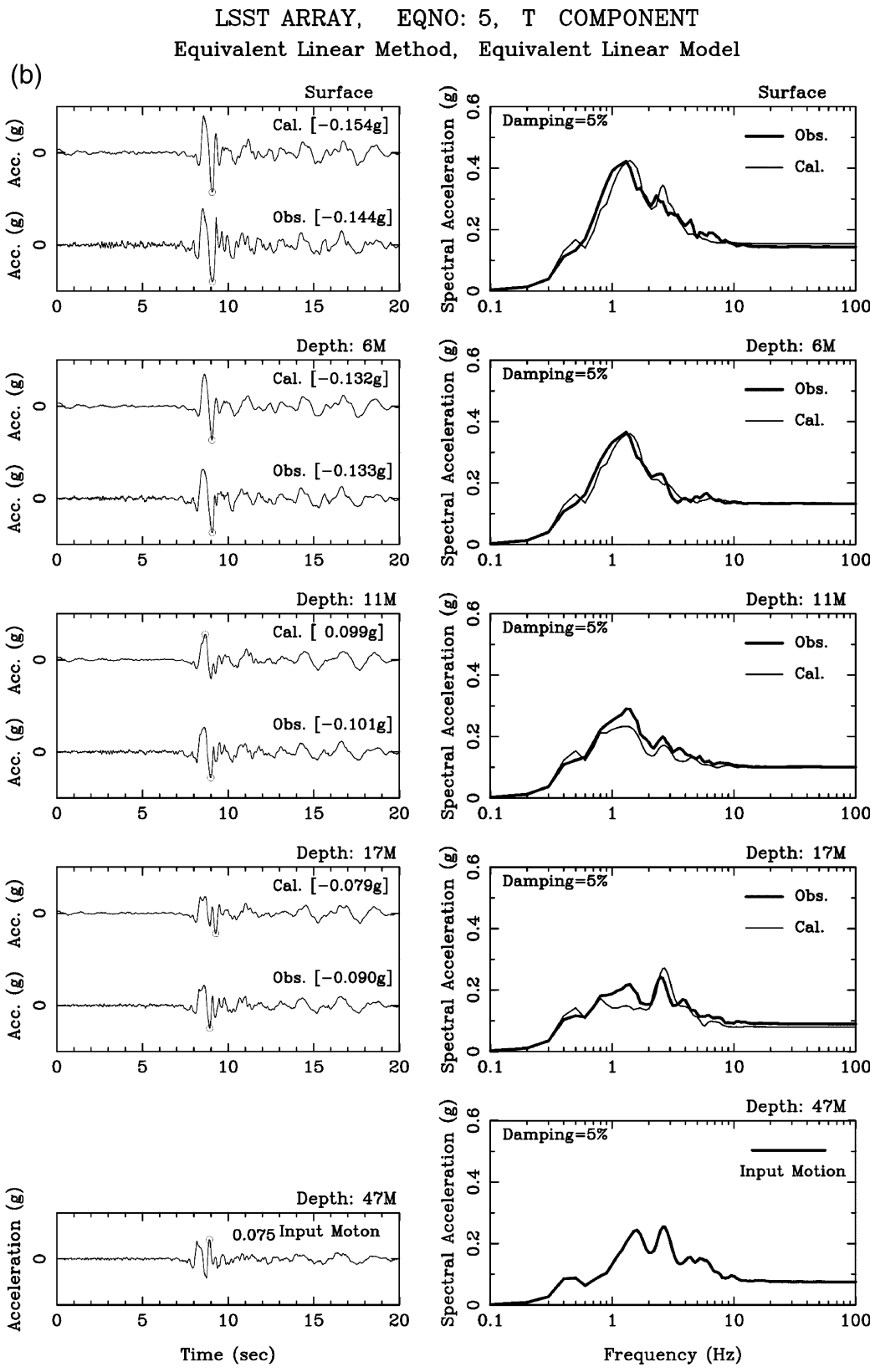

Fig. 5 (*continued*)

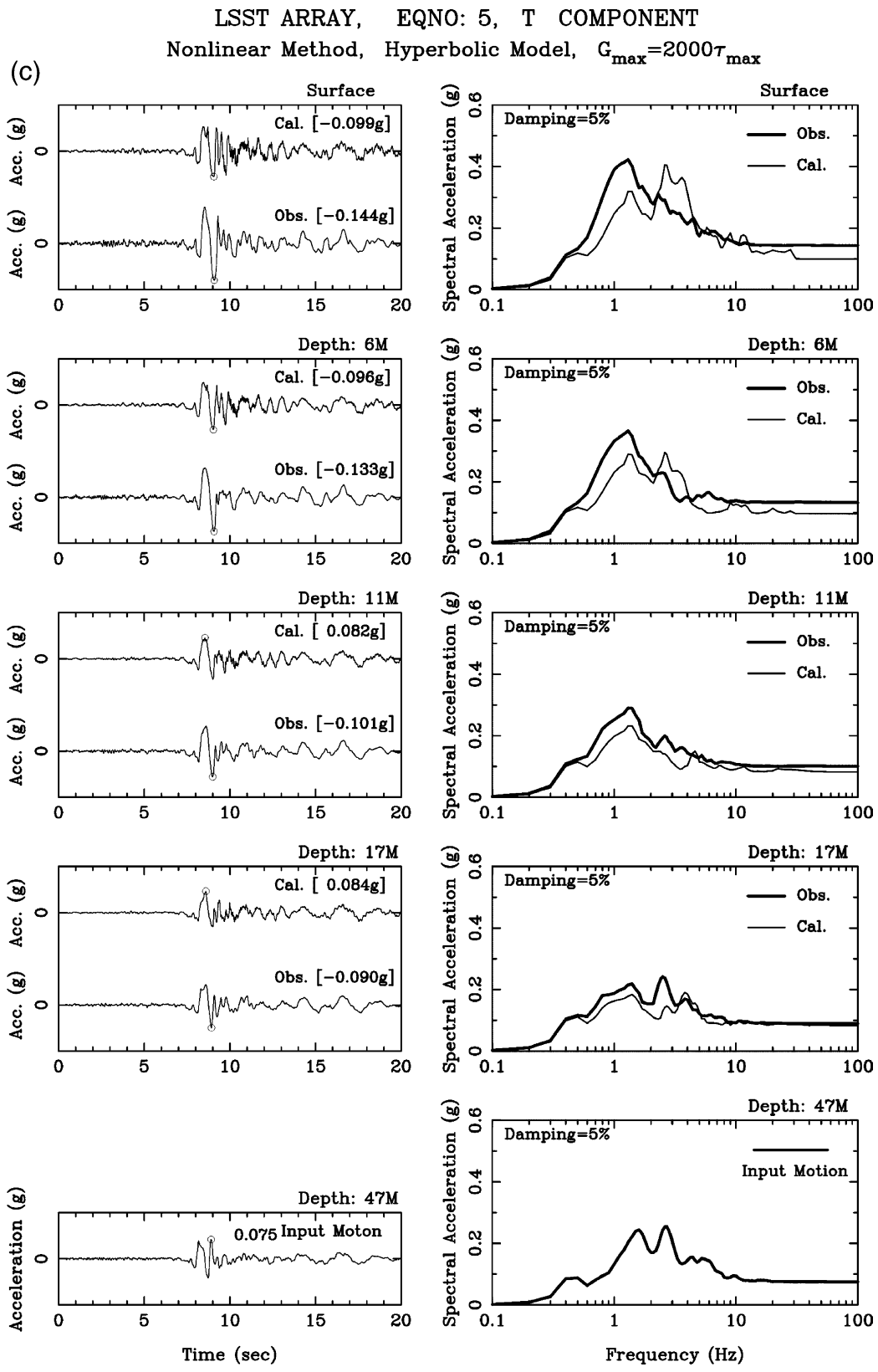

Fig. 5 (*continued*)

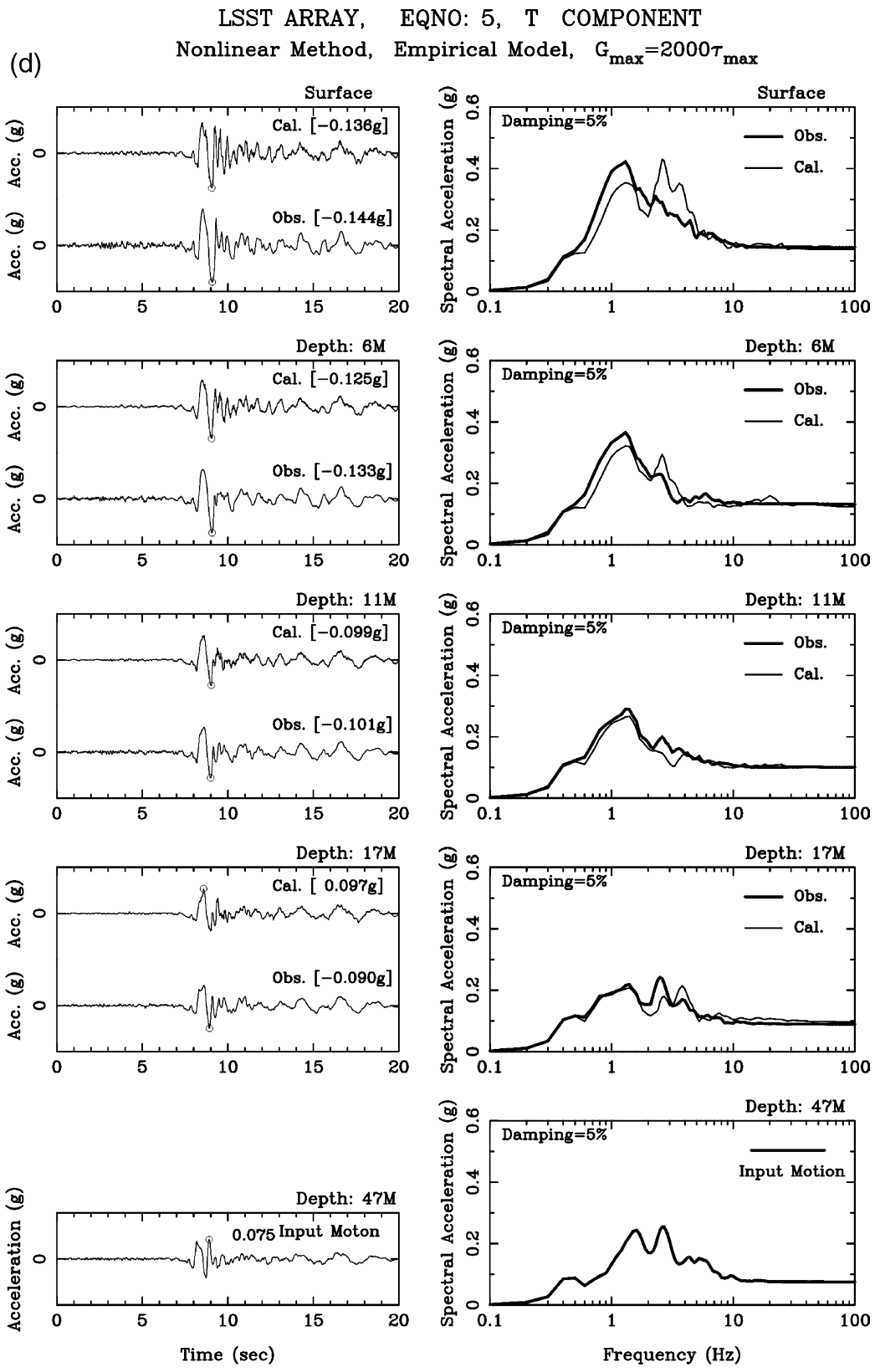

Fig. 5 (*continued*)

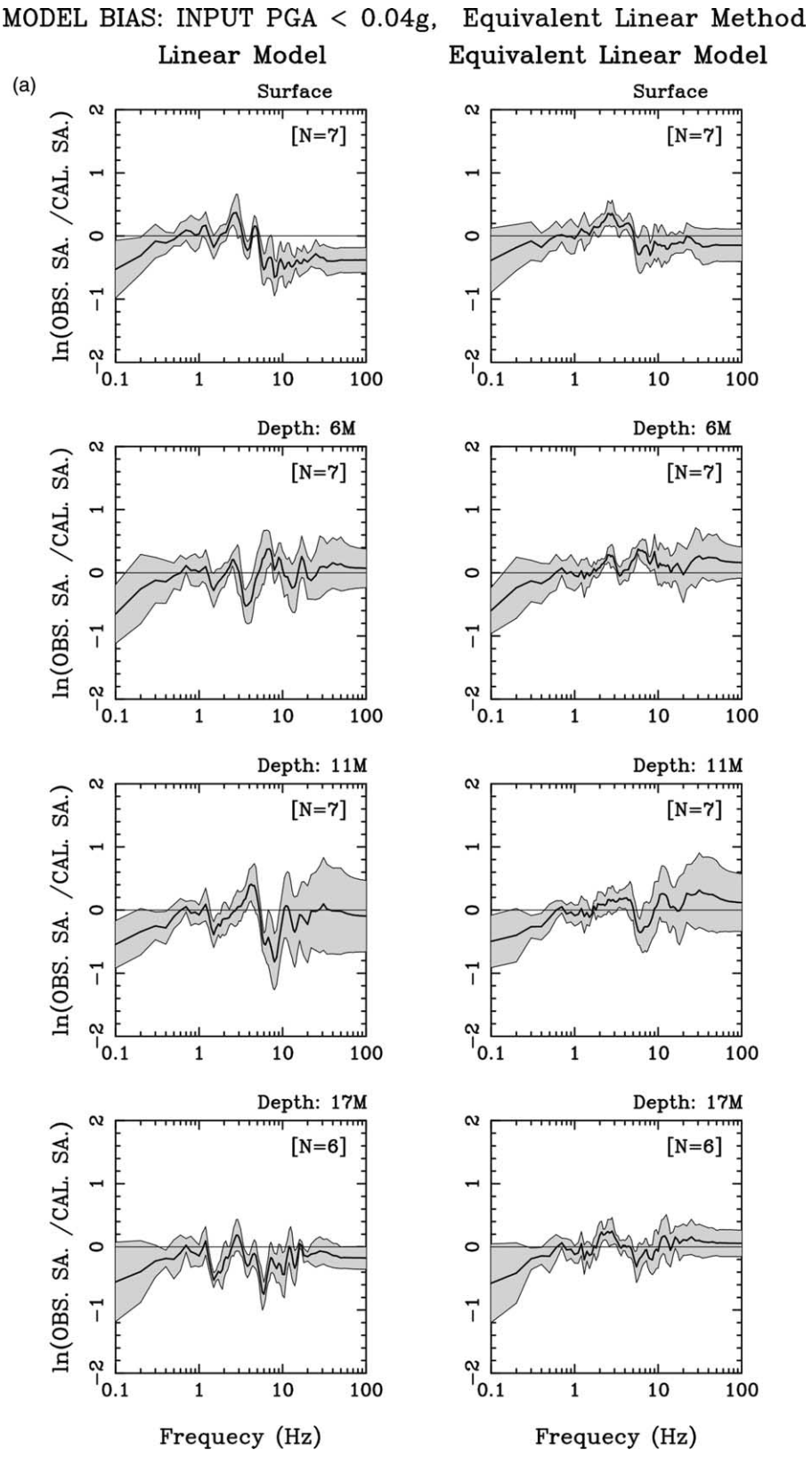

Fig. 6. (a) Model bias of the seven small input motions (PGA < 0.04 g) using the equivalent-linear method with the linear and equivalent-linear models. (b) Model bias of the seven small input motions (PGA < 0.04 g) using the nonlinear method with the linear, hyperbolic, and empirical models. (c) Model bias of the six large input motions (PGA > 0.04 g) using the equivalent-linear method with the linear and equivalent-linear models. (d) Model bias of the six large input motions (PGA > 0.04 g) using the nonlinear method with the linear, hyperbolic, and empirical models.

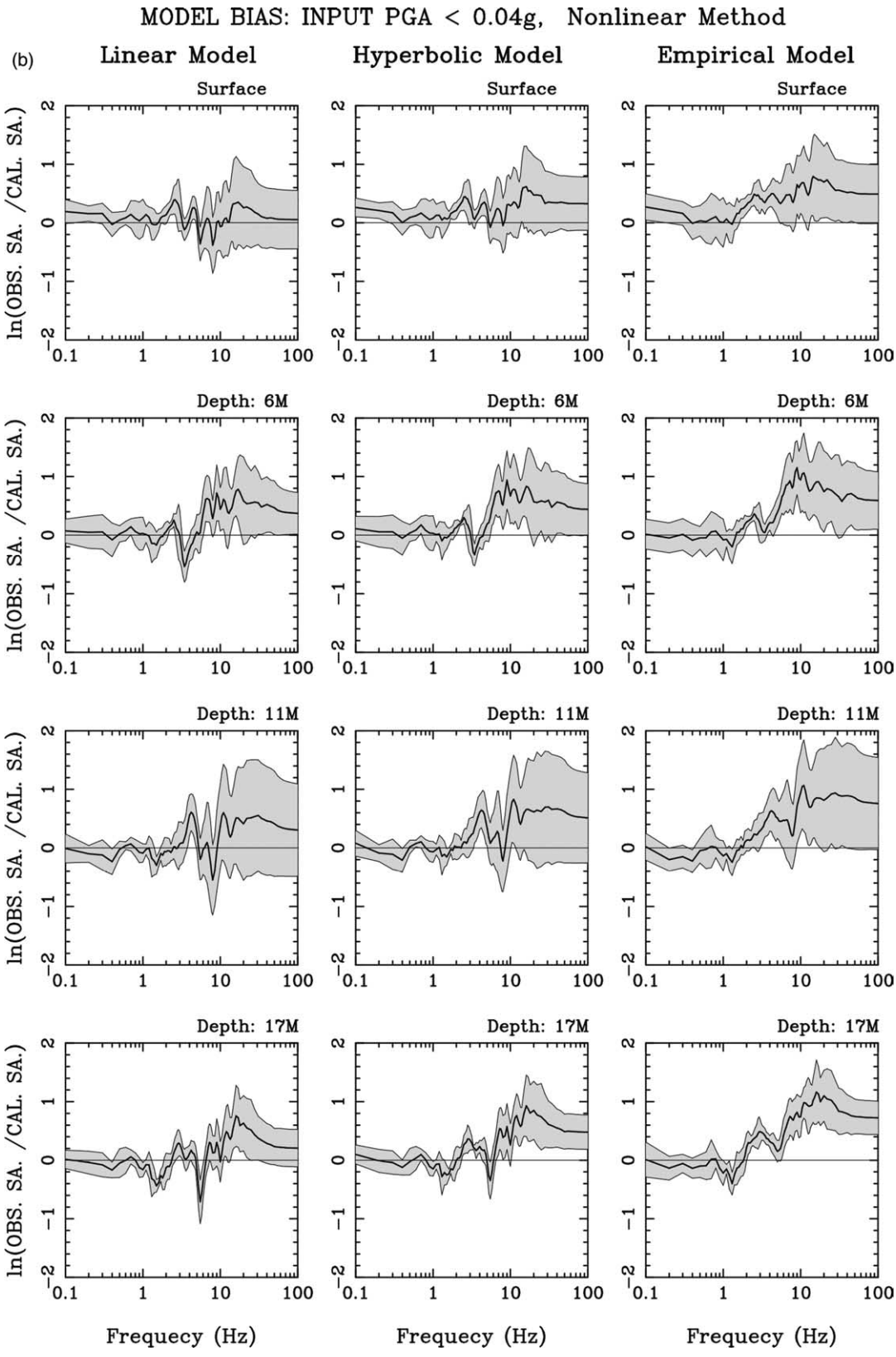

Fig. 6 (*continued*)

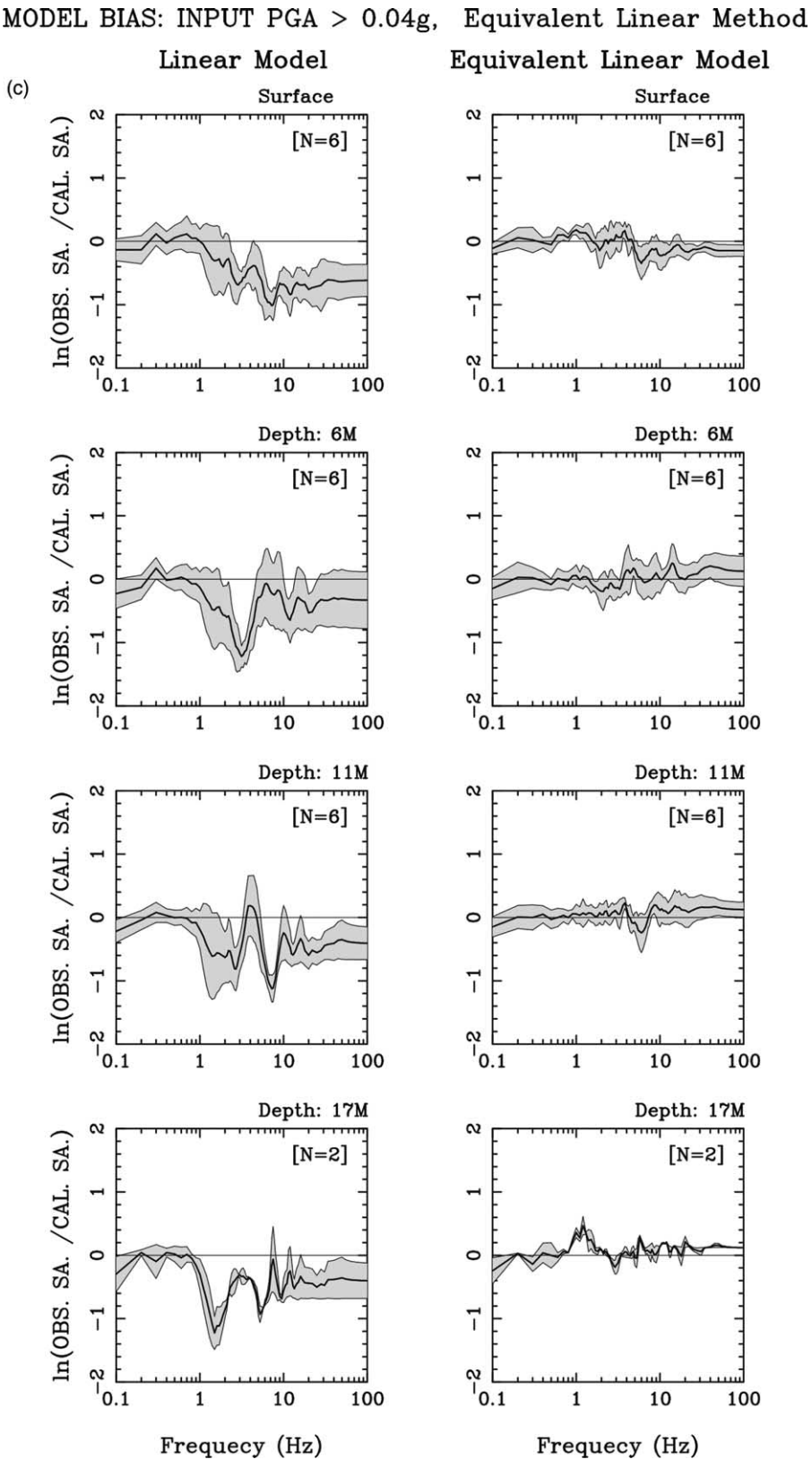

Fig. 6 (*continued*)

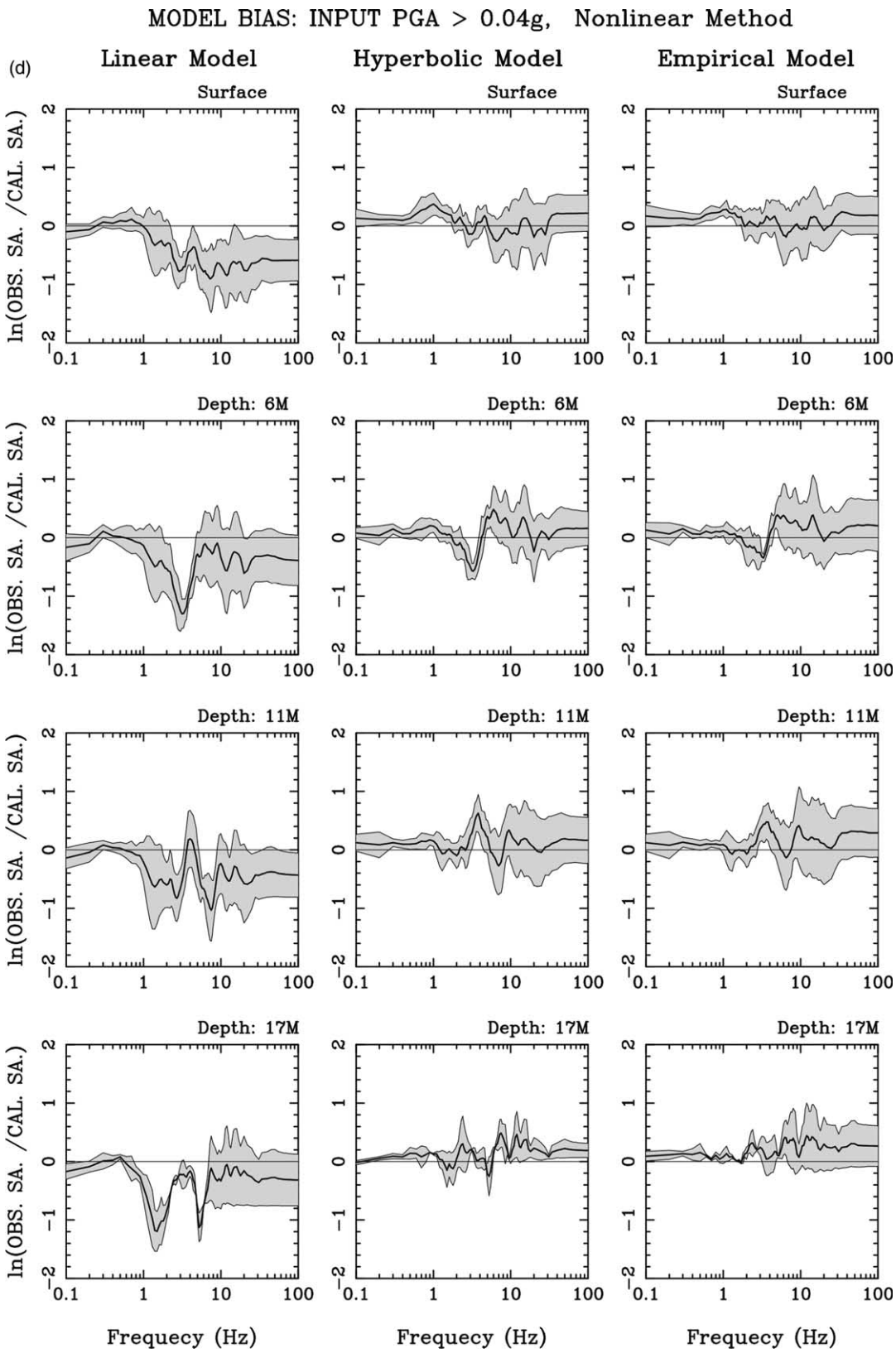

Fig. 6 (*continued*)

earthquakes with input motions larger than 0.04 g are classified as strong events. We then compare the differences between the observed records and the calculated records by different models.

Fig. 6a shows the resultant deviation obtained by the equivalent-linear method of seven weak motions. The left hand side shows the deviation from the linear model and the right hand side shows the deviation from the equivalent-linear model. The deviation in this figure is defined as the logarithm of the ratio between the observed and calculated spectra. The deviation is shown for points on the surface and at the depths 6, 11 and 17 m, respectively, from top to bottom of this figure. The solid line represents the mean values and the shaded band represents plus and minus one standard deviation from mean value. The N value in each frame represents the number of records. The N values at 17 m are less than others, because of lack of records or using the record as input motion. In general, the results from the two models are consistent, with the equivalent-linear model being slightly better. The mean values are close to the zero line and the variations are small. On the surface, records obtained from the linear model are slightly greater than the observed at high frequencies.

The model deviations between the observed and calculated records at different depths using three models in the nonlinear method for the 7 weak motions are shown in Fig. 6b. On the left hand side, middle and right hand side are results from the linear model, hyperbolic model and empirical model, respectively. The mean values of the three models are close to zero for the low frequencies, but the deviations above 10 Hz are significantly greater than the deviations in the equivalent-linear method (Fig. 6a). The model deviation greater than zero means underestimation. Generally speaking, the results by the equivalent-linear and nonlinear methods are in excellent agreement between 0.1 and 10 Hz. The mean values are negative at the depths 6, 11, and 17 m near 1.2 Hz. And the mean values in both linear models are negative at the depth 17 m near 6 Hz, the depth 11 m near 8 Hz, and the depth 6 m between 3 and 4 Hz. This shows that overestimation presented in the same frequency band by different methods is influenced by the soil properties.

Fig. 6c represents the result from two models of the equivalent-linear method for the six strong input motions. The mean values from the linear model are obviously below zero at high frequencies in the left hand side of the figure. And the mean value of the equivalent-linear model is still near zero. This implies that the results from the linear model are significantly greater than the observed, whereas the results from the equivalent-linear model match well with the observed.

The same results are also obtained by the nonlinear method, as shown in Fig. 6d. In the left hand side, the mean values from the linear model are obviously negative and are the same as the results from linear model by the equivalent-linear model. But the mean values are still close to zero in hyperbolic and empirical models. We conclude that for large input motions the results from these two models are consistent with the observed, and the results from linear model clearly show overestimation. The model deviations of nonlinear method are lager than the equivalent-linear method in Fig. 6a–d. It may be caused by the difference of methods. The equivalent-linear method calculated in frequency domain is more stable than the nonlinear method calculated in time domain.

Table 4
Goodness of fitting with weak and strong input motions for different models

Method	Equivalent-linear method		Nonlinear method		
Model	Linear	Equival-ent-linear	Linear	Nonlinear	
				Hyper-bolic	Empirical
Weak motion	O	O	O	X	X
Strong motion	X	O	X	O	O

O, good fitting; X, poor fitting.

The results from both weak and strong input motions are summarized in Table 4. These results of all 13 earthquakes show that the soil profile and shear modulus reduction curve are stable and reliable. Based on above results, we can say that the synthetic records obtained from linear model match well with the actual records for small input motions. The computed records obtained from the equivalent-linear model are consistent with the observed records. But the results obtained from the hyperbolic and empirical models by nonlinear method show underestimation. These results prove that the computed records are reliable in the linear regime of soil properties and by two kinds of one-dimensional synthetic method we used. Therefore, the synthetic records obtained from linear model will overestimate proportionally when the input motion increases. The results obtained from the equivalent-linear model and nonlinear model are in good agreement with the served records. In conclusion, nonlinear soil response has taken place in the DHB hole of the LSST array when the recorded PGA value exceeded 0.04 g.

5. Discussion

5.1. Transfer function

In general, the transfer function is calculated as the ratio of one pair of Fourier spectra. Fig. 7 shows the spectral ratio of the surface and bottom acceleration waveforms by the Fourier spectrum (in red) and by the spectral acceleration with zero damping (in green) and with 5% damping (in blue). The Fourier spectral ratio (red curve) is only plotted from 0.1 to 5 Hz, because the ratio is unstable in higher frequencies (i.e. due to small value being divided by small value). We can find the dominant frequencies of the Fourier spectral ratio and spectral acceleration ratio with both zero and 5% damping are very consistent. Although the 5%-damping spectral acceleration ratio is reduced in its amplification, the dominant

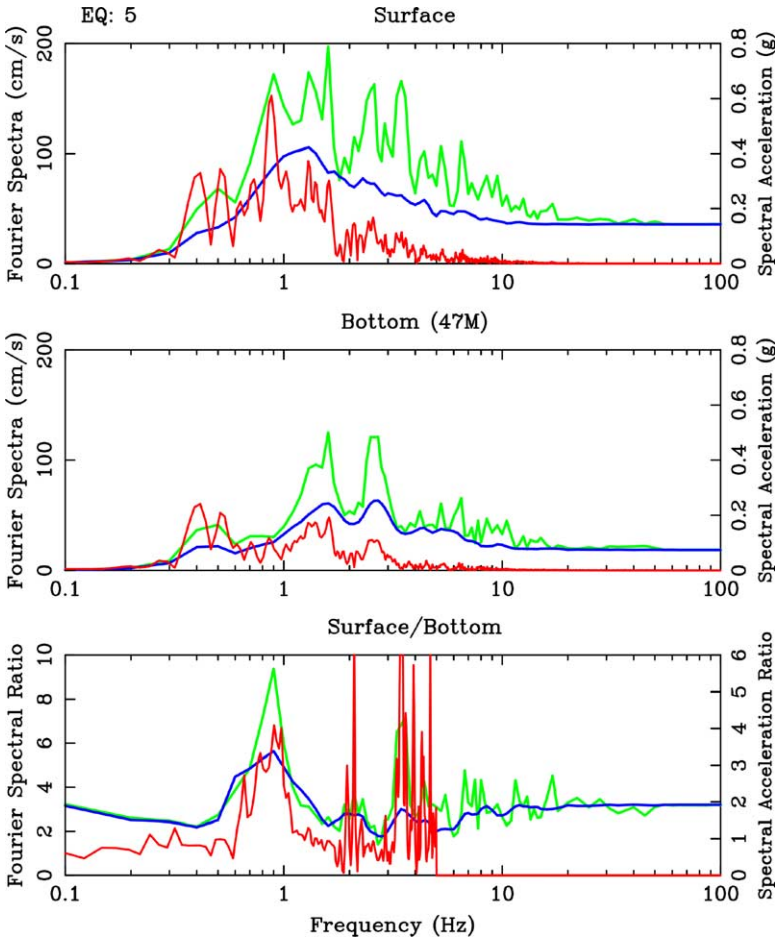

Fig. 7. Comparison of the Fourier spectrum and response spectrum (SA) for EQ5. The red, green, and blue curves denote the Fourier spectrum, spectral acceleration response spectrum with zero-damping, and with 5%-damping, respectively. The upper figure shows the spectra of acceleration on the surface. The middle figure shows the spectra of acceleration at depth of 47 m. The bottom figure shows the spectral ratio of the surface and bottom records. The Fourier spectra ratio is shown only from 0.1 to 5 Hz.

frequency is still prominent. Therefore, the spectral acceleration ratio can be used to identify the dominant frequency.

Based on above results of comparing the Fourier spectral ratio and spectral acceleration ratio, we now proceed to use the spectral acceleration ratio between the surface and bottom records as the transfer function. The spectral acceleration ratios of the surface and bottom records at the small input level of the four pairs are shown in Fig. 8a. The black curve means the spectral ratio of the observed surface record and observed bottom record in transverse component. The red, green, blue, and cyan curves represent the spectral ratio of the surface records computed from the linear model and equivalent-linear model by the equivalent-linear approach, from the hyperbolic model and empirical model by the nonlinear method, respectively, with respect to the same observed bottom records in transverse component.

In general, the results computed by all models were consistent with the observed record between 1 and 10 Hz. We find that the calculated records obtained from the linear model of equivalent-linear method significantly overestimate in high frequency in A, B, and C of Fig. 8a. The records obtained from the equivalent-linear model match well with the observed record. But the results obtained from the hyperbolic and empirical models underestimate, especially in high frequencies. In D of the figure, the records of all models are greater than the observed at frequencies above 3 Hz. The dominant frequencies of the observed and calculated results are between 1 and 2 Hz in input motion at 47 m depth of A, B, and C. The dominant frequencies of the observed and calculated records are about 3 Hz in the input motion at 17 m depth of D.

The response spectral ratios for large PGA values in the four pairs are shown in Fig. 8b. The calculated results of linear model again overestimate above 2 Hz in A and D, and obviously overestimate above 1 Hz in B and C. The calculated records of other models match well with the observed records. We can conclude that the results of the linear model cannot match the observed records when input PGA value is greater than 0.04 g. In other words, the nonlinear ground response has taken place in the soil layers. Moreover, the nonlinear effects are unequivocal when the PGA value reaches 0.075 g. When the input motion is at depth 17 m in A and D, the dominant frequency of the linear model in the equivalent-linear method is near 3 Hz, other models are lower. The fundamental frequency is shifted to lower frequency in the observed record

in all models except the linear model. When the input motions at depth 47 m in B and C groups are larger than 0.04 g, the fundamental frequency of the linear model in the equivalent-linear method is between 1 and 2 Hz. But the observed dominant frequency and other calculated results clearly shift to a lower frequency and the amplitude ratio also decreases.

5.2. The relation of stress and strain at different depths

We also calculated the relation of stress and strain at different depths, and examine the soil behaviors in all layers. The relations of stress and strain computed by the nonlinear method at different depths for the low-level shaking earthquake, EQ6, are shown in Fig. 9a. From top to down, the stress–strain relations are for points on the surface and at depths of 6, 11, and 17 m, respectively. The left and right hand sides show the results generated during the time interval 1.5–5 and 5–15 s, respectively. The left hand side represents the primary portion of the record in the time history. And the right hand side represents the coda portion of the record in the same time history. The solid line represents stress–strain relation computed by empirical model, and dash line represents the result from the linear model. We can see that the difference is not obvious between the empirical and linear models for weak motions.

In Fig. 9b, the stress–strain relation of empirical model develops a hysteresis loop during the primary portion of strong motion EQ5. The maximum strain was about 0.09% at depth 11 m. Then the soil returns to the linear regime right after the primary portion of time history. But a permanent strain of about 0.01% occurred at depth 11 and 17 m at the end of the record. In the meantime, the hysteresis loops also deviate from

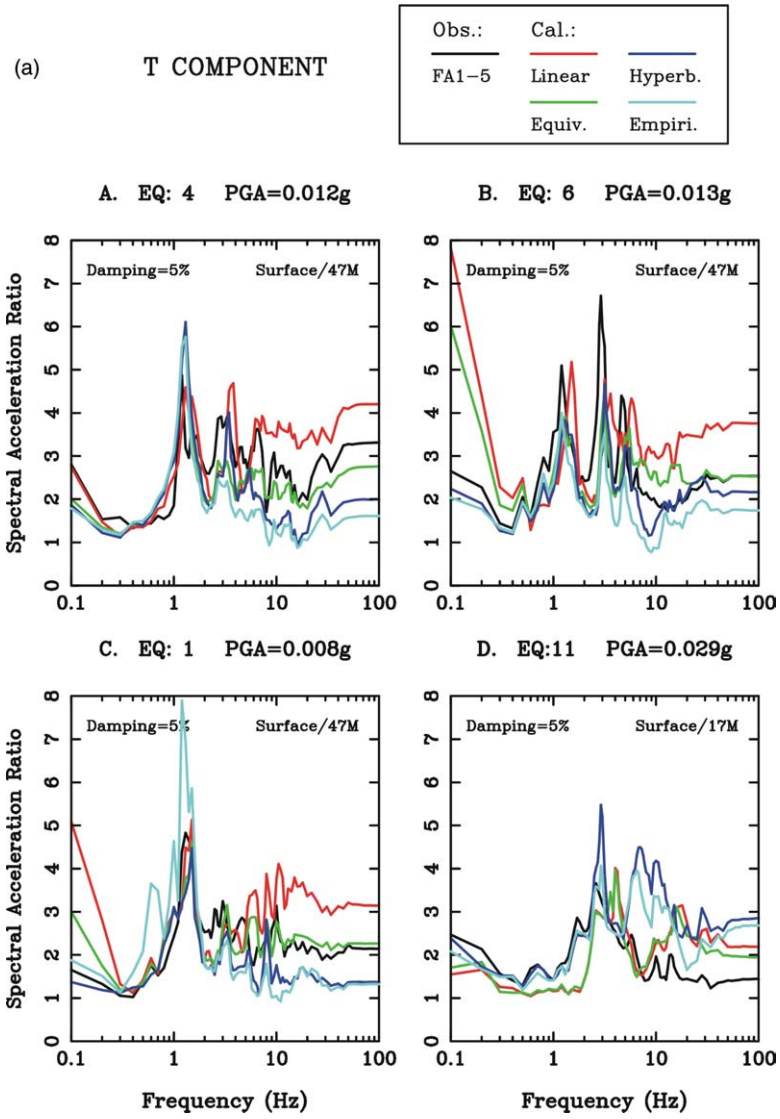

Fig. 8. (a) Spectral acceleration ratio for small PGA in the four groups. Black, red, green, blue, and cyan curves represent the spectral ratio of the observed surface record, surface records computed from the linear model and equivalent-linear model by the equivalent-linear approach, from the hyperbolic model and empirical model by the nonlinear method, respectively, and the observed bottom records. (b) Spectral acceleration ratio for large PGA in four groups.

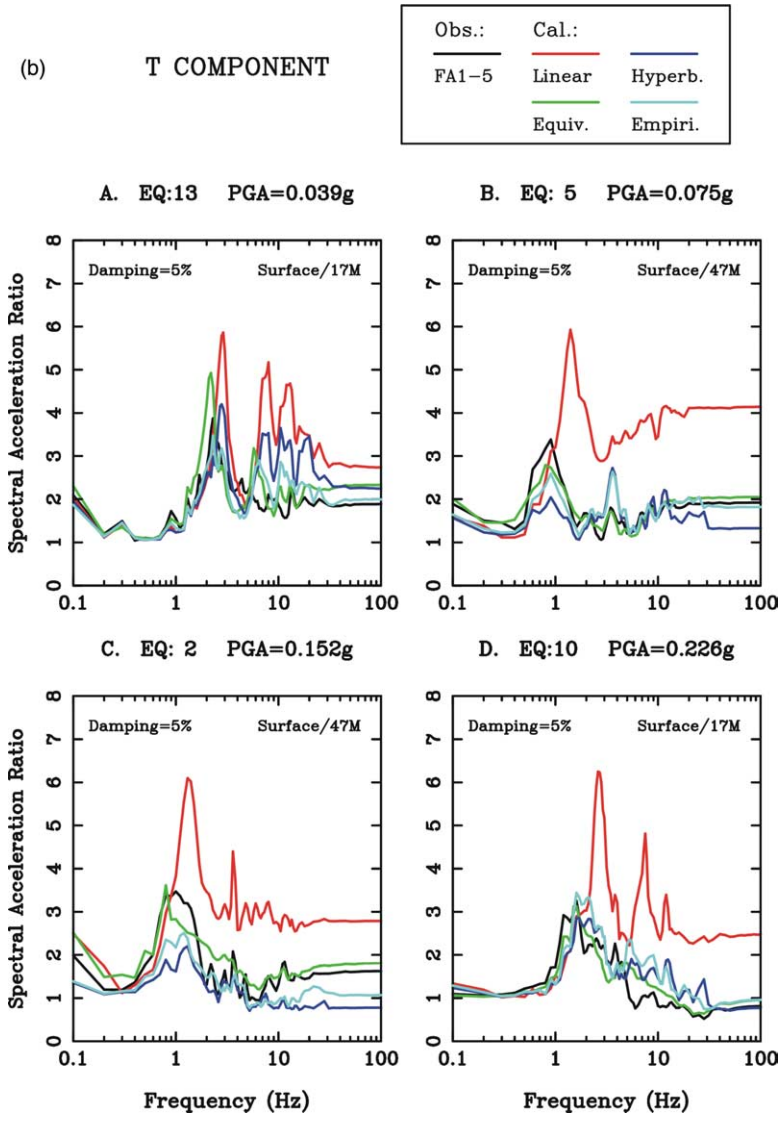

Fig. 8 (*continued*)

the origin. The slope (i.e. shear modulus) of stress–strain relation from empirical model is also decreased compared to linear model.

The resonance frequency increases in the coda portion after the primary portion of the record, indicating that the site response during the weaker motion of the coda has recovered to be linear following the primary *S* wave [8,24]. The hysteresis loop of EQ5 shows similar result, because the shear modulus G_{max} is proportional to *S* wave velocity.

5.3. The observed nonlinearity in the time and frequency domains

We can find the nonlinearity from the accelerations of LSST array both in the time and frequency domains. By comparing the PGA between the bottom and at different depths, we obtain the amplification of the ground motion. The relations of PGA at 47 m bottom and PGA on the surface, 6, 11, and 17 m for nine earthquakes are shown in Fig. 10a. In the lower right plot, the PGA at 17 m versus the bottom PGA show a one to one linear relation. In the lower left plot, the PGA at 11 m versus the bottom PGA are still close to one to one linear relation, even in the high PGA at the bottom. In the upper right plot, the PGA values start to move to one to two relation at 6 m, and the low PGA at 6 m in response to high PGA at the bottom shows clearly deamplification. In the upper left plot, the two times PGAs on the surface with respect to the bottom show the free surface effect. The shaded zones represent the bottom PGAs from 0.04 to 0.075 g. It marks the transition range in which deamplification started to occur. Four earthquakes with 17 m bottom PGA are show in Fig. 10b. In the lower left plot, the one to one relation is shown at 11 m. Then deamplification is shown obviously at 6 m for high bottom PGA of about 0.23 g, as shown in the upper right plot. The doubling of PGA is also shown on the surface for free surface effect. The nonlinearity appears at shallow depth. From above results we can conclude

that the free surface effect controls the amplification on the surface. The nonlinearity begins to occur when the input PGA exceeded 0.04 g, and is unequivocal at 0.075 g. The nonlinear soil layer is at the depths between 6 and 17 m.

In frequency domain, the dominant frequencies of response spectral ratios from observed records (black curves) between surface and bottom motions for weak and strong bottom motions in Fig. 8 show unequivocal nonlinearity. When we compare the dominant frequencies of the B, C, and D pairs between weak and strong motions in Fig. 8a and b, we find the peaks shift toward lower frequencies to about 0.3, 0.3, and 1.0 Hz for the B, C, and D pairs, respectively. The spectral ratios also decrease to about 1.7, 1.4, and 0.4 for the B, C, and D pairs, respectively. It is noted that the dominant frequencies are different in pair A, because the two bottom motions are at different depths. The shifted frequency and decreased amplitude clearly show nonlinearity in the soil layers.

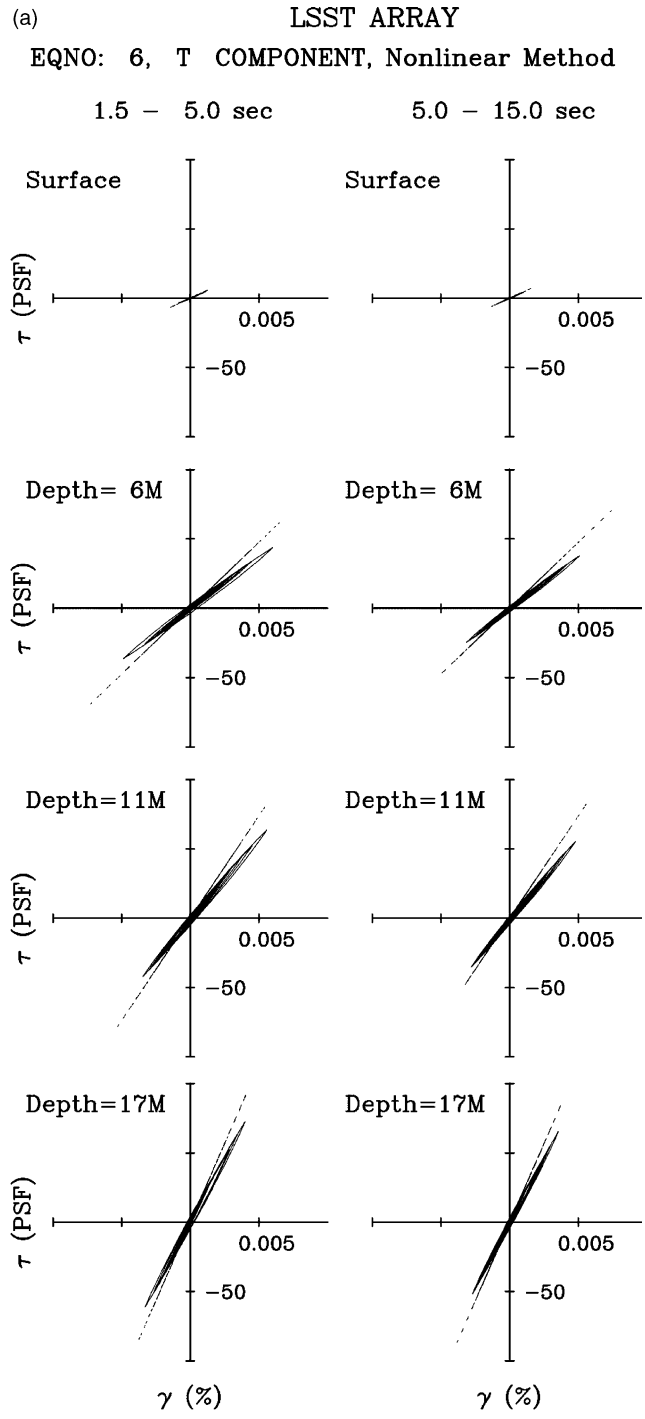

Fig. 9. (a) The hysteresis loops at different time windows and depths by EQ6. The dash and solid lines represent stress–strain relation computed by the linear and empirical model, respectively, of the nonlinear method. (b) The hysteresis loops at different time windows and depths by EQ5.

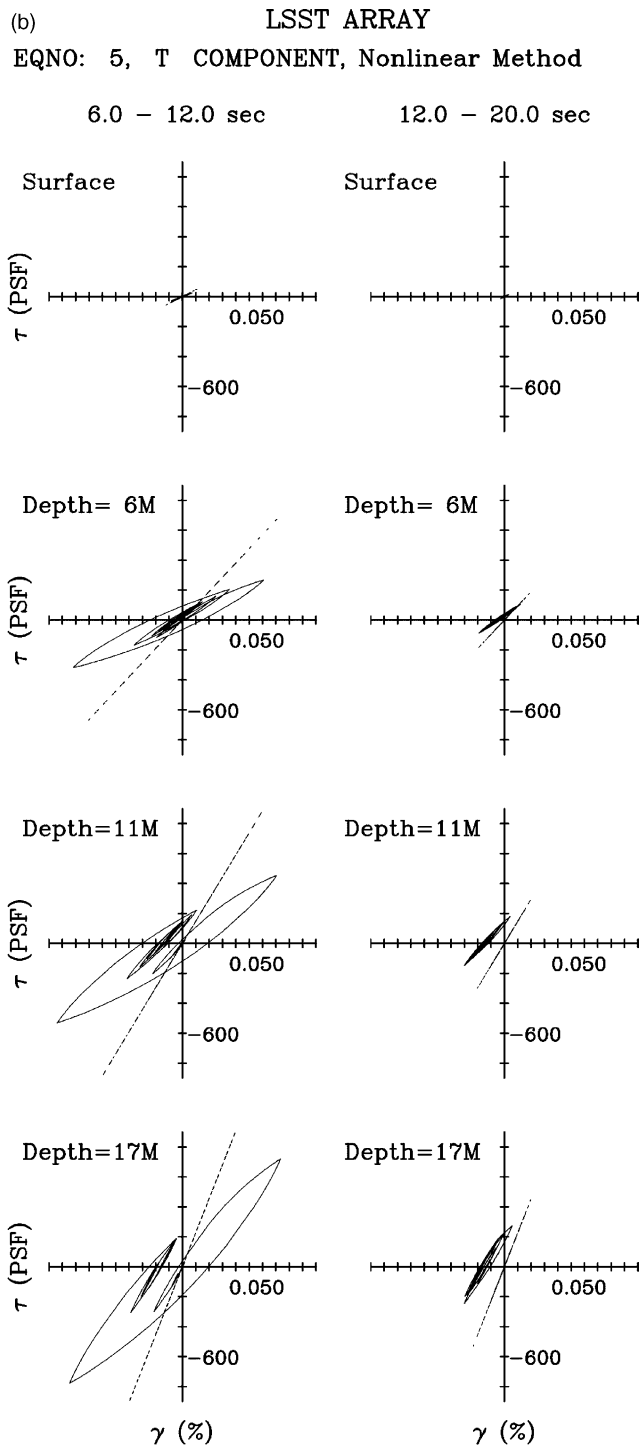

Fig. 9 (*continued*)

Previous research results by other researchers also reported the shift of spectral peaks toward longer periods progressively with increasing ground motion. For example, Trifunac and Todorovska [25] found the period and amplitude changes of local peaks in the Fourier amplitude spectra of free-field strong ground motion recorded at five stations in San Fernando Valley, Los Angeles. The results suggest that the local peaks reoccur during shaking by small local earthquakes with peak ground velocity, $v_{max} < 10$–20 cm/s. The peaks shifted toward longer periods during large strong motion amplitudes, $v_{max} > 20$ cm/s. Moreover, they [2] found nonlinear response of soil begins to distort the amplification factors determined from small amplitude in the epicentral area of the Northridge earthquake of 1994 when the peak ground velocities are larger than $v_m \approx 15$ cm/s. The site response becomes progressively more affected by the nonlinear soil response when moving into

the area of near-field and strong ground motion, $v_m > 30$ cm/s. Trifunac and Ivanović [26,27] present the period shift and amplitude change and the reoccurrence of local peaks in the Fourier amplitude spectra of strong ground motion in former Yugoslavia. The data suggest that some local peaks reoccur during shaking by small local earthquakes with peak ground velocity, $v_{max} < 10$–20 cm/s. During large strong-motion amplitudes ($v_{max} > 20$ cm/s), the peaks are shifted toward longer periods or disappear. In summary, those results also show the presence of a threshold of ground shaking between linear and nonlinear soil response.

6. Conclusions

The soil properties in real world are complex. The nonlinearity of the LSST site was found previously by analyzing the observed data [6,7] and simulating the earthquake series of 20 May 1986 [28–33]. In this study, we reconstructed a simple layer model based on soil tests and well logging data. We computed simultaneously the ground response in each layer by both the one-dimensional equivalent-linear and nonlinear methods using records of the LSST downhole arrays from 13 earthquakes. We then compared the synthetic with the observed records. The results of the 13 earthquakes show that the soil profile and shear modulus reduction curve are stable and reliable.

We divide the data of 13 earthquakes into four groups according to their epicentral locations. It is not easy to find the difference of waves arriving from different directions because the incident waves are almost perpendicular to the surface in the very shallow layers. We focus on comparing the difference of amplitude and frequency between the bottom and top layers, because the frequency contents of input motion can affect the soil nonlinearity.

We found that the calculated records in the linear model and observed records match well at weak motions from seven earthquakes. The calculated records obtained from the equivalent-linear model are also consistent with the observed. But the results from hyperbolic and empirical models by the nonlinear method tend to underestimate. These results prove that

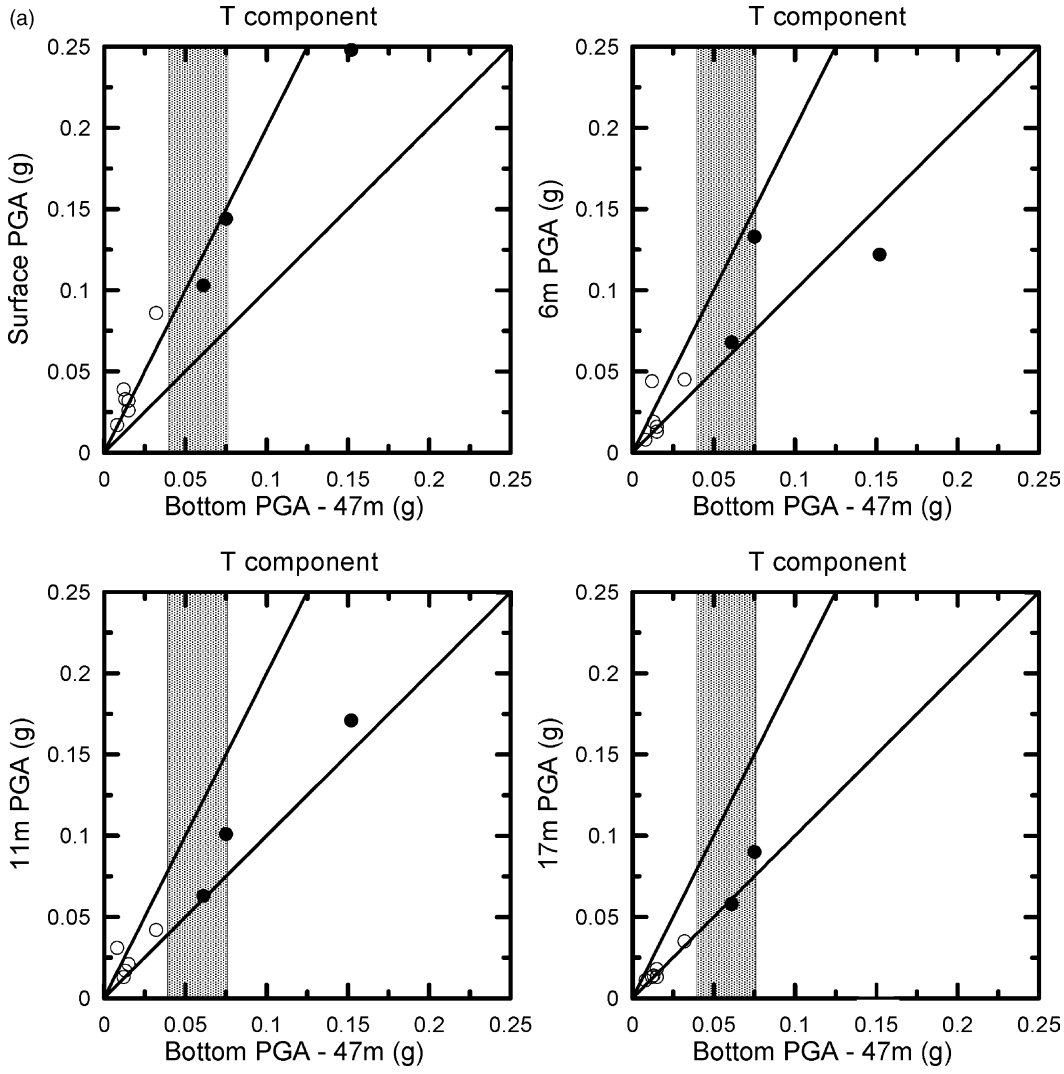

Fig. 10. (a) The relation of bottom PGA and the PGA at different depths. The white and black circles denote the weak input motion and strong input motion, respectively. The bottom is at 47 m. (b) The relation of bottom PGA and the PGA at different depths. The bottom is at 17 m.

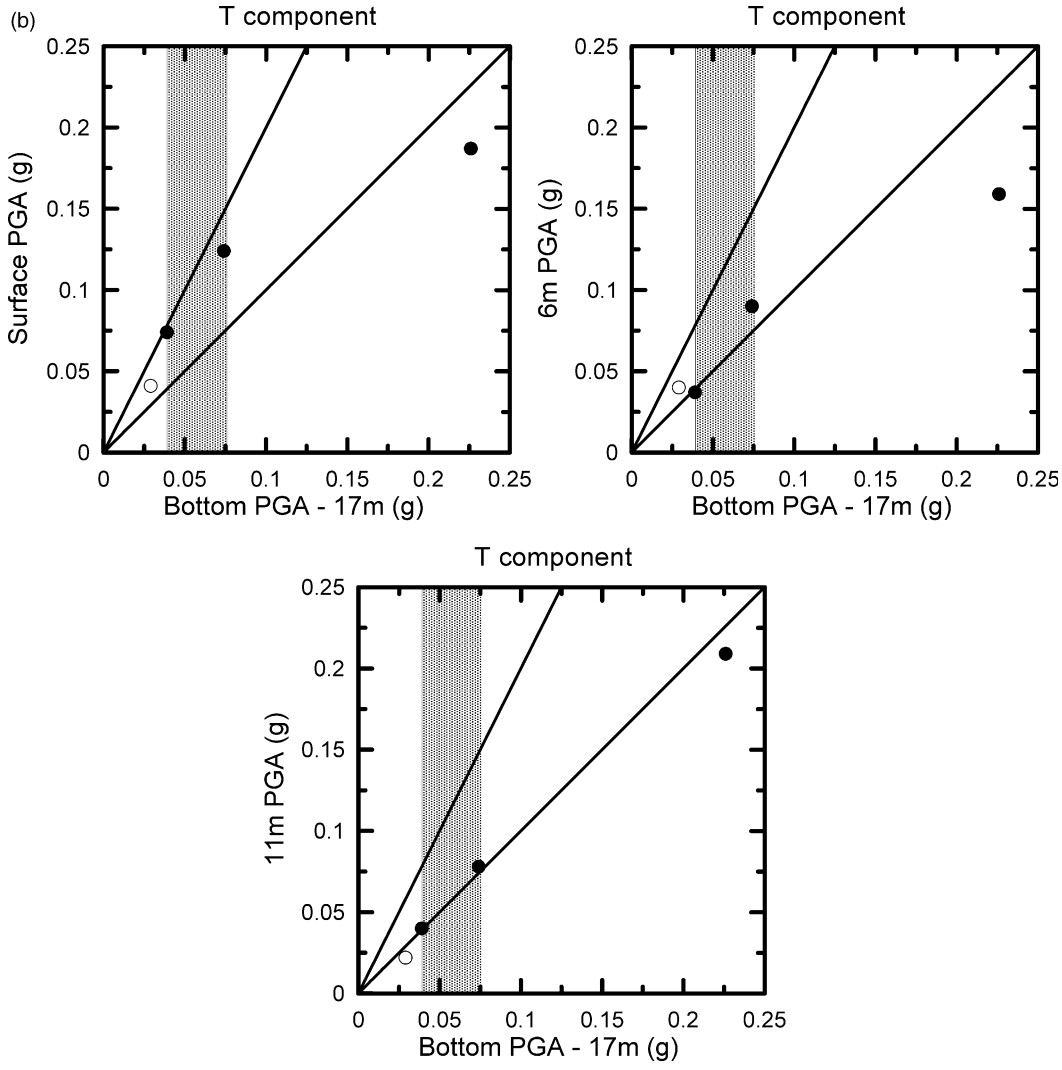

Fig. 10 (*continued*)

the calculated records are reliable in the linear regime of soil properties and by the two kinds of one-dimensional method we used.

For strong motions from the other six earthquakes, the results from linear model are obviously overestimated. The calculated records obtained from the equivalent-linear model, hyperbolic model, and empirical model are in excellent agreement with the observed records. This shows that the computed records obtained from the equivalent-linear and nonlinear models can provide good synthetic results. The observed records from these earthquakes have shown nonlinear soil response. By the nonlinear method, we further computed the hysteresis loops at high level of shaking and found a permanent strain change of about 0.01% at depth 11 and 17 m.

The soil nonlinearity can also be caused by the site conditions [24,34]. According to previous site classification [35], the LSST site belongs site class D. The soil condition of LSST site is very soft. The star marks the location of seismic sensor corresponding to the layer in Table 2. All of the layers with seismic sensors are sand. The shear wave velocities in the layers at depths of 6 and 11 m do not show anomalously low values, but the density seems a little low in these layers. From the observed results, we can find the nonlinearity began at a bottom (47 m) PGA of 0.04 g, and became unequivocal at the bottom PGA of 0.075 g in the LSST site. In comparison with the amplification of the SMART1 array around the LSST site, the results show deamplification when the PGA exceeds 40 gal [6]. Based on the results obtained in this study, we can reliably estimate the ground motions at depth by the equivalent-linear and nonlinear methods with the soil profile and reduction curves in the LSST site.

Acknowledgements

We are grateful to Dr B.H. Chin for his helpful discussions and suggestions. We thank the Institute of Earth Sciences, Academia Sinica for providing the strong motion records of the LSST array. We also thank an anonymous reviewer for useful

comments and suggestions. The research was supported by the National Science Council, Republic of China, under the Grant NSC 92-2625-Z-008-011 and NSC 94-2116-M-008-005.

References

[1] Aki K, Richards PG. Quantitative seismology theory and methods. vol. 1. New York: W.H. Freeman; 1980.
[2] Trifunac MD, Todorovska MI. Can aftershock studies predict site amplification factor? Northridge, CA, earthquake of 17 January 1994. Soil Dyn Earthq Eng 2000;19:233–51.
[3] Seed HB, Idriss IM. The influence of soil conditions on ground motions during earthquake. J Soil Mech Found Eng Div ASCE 1969;94:93–137.
[4] Chin BH, Aki K. Simultaneous determination of source, path and recording site effects on strong ground motion during the Loma Prieta earthquake—a preliminary result on pervasive non-linear site effect. Bull Seismol Soc Am 1991;81:1859–84.
[5] Aki K. Local site effects on weak and strong ground motion. Tectonophysics 1993;218:93–111.
[6] Wen KL. Nonlinear soil response in ground motions. Earthq Eng Struct Dyn 1994;23:599–608.
[7] Wen KL, Beresnev IA, Yeh YT. Investigation of nonlinear site amplification at two downhole strong ground motion arrays in Taiwan. Earthq Eng Struct Dyn 1995;24:313–24.
[8] Satoh T, Sato T, Kawase H. Nonlinear behavior of soil sediments identified by using borehole records observed at the Ashigara Valley, Japan. Bull Seismol Soc Am 1995;85:1821–34.
[9] Satoh T, Horike M, Takeuchi Y, Uetake T, Suzuki H. Nonlinear behaviour of scoria soil sediments evaluated from borehole records in eastern Shizuoka prefecture, Japan. Earthq Eng Struct Dyn 1997;26: 781–95.
[10] Aguirre J, Irikura K. Nonlinearity, liquefaction, and velocity variation of soft soil layers in Port Island, Kobe, during the Hyogoken-Nanbu earthquake. Bull Seismol Soc Am 1997;87:1244–58.
[11] Jarpe SP, Cramer CH, Tucker BE, Shakal AF. A comparison of observations of ground response to weak and strong ground motion at Coalinga, California. Bull Seismol Soc Am 1988;78:421–35.
[12] Jarpe SP, Hutchings LJ, Hauk TF, Shakal AF. Selected strong- and weak-motion data from the Loma Prieta earthquake sequence. Seismol Res Lett 1989;60:167–76.
[13] Darragh RB, Shakal AF. The site response of two rock and soil station pairs to strong and weak ground motion. Bull Seismol Soc Am 1991;81: 1885–99.
[14] Steidl JH, Tumarkin AG, Archuleta RJ. What is a reference site? Bull Seismol Soc Am 1996;86:1733–48.
[15] Chen CH, Huang JH, Chen LY. Comparison of geological profiles obtained from different exploration methods. Bull Coll Eng NTU 1990; 49:31–48.
[16] HCK. Geophysical survey report of Lo-Tung project for Taiwan Power Company. HCK Geophysical Company; 1986.
[17] Chang CY, Mok CM, Power MS, Tang YK, Tang HT, Stepp JC. Equivalent linear versus nonlinear ground response analyses at Lotung seismic experiment site. In: Proceedings of the fourth US national conference on earthquake engineering, Palm Springs, California, vol. 1; 1990, p. 327–36.
[18] Seed HB, Idriss IM. Soil moduli and damping factors for dynamic response analysis. Report No. EERC70-10, University of California, Berkeley; 1970.
[19] Schnabel PB, Lysmer J, Seed HB. SHAKE: a computer program for earthquake response analysis of horizontally layered sites. Report No. EERC72-12, University of California, Berkeley; 1972.
[20] Joyner WB, Chen ATF. Calculation of nonlinear ground response in earthquakes. Bull Seismol Soc Am 1975;65:1315–36.
[21] Lam I, Tsai CF, Martin GR. Determination of site dependent spectra using nonlinear analysis. Second international conference on microzonation, San Francisco, California; Nov. 1978.
[22] Konder RL, Zelasko JS. A hyperbolic stress-strain formulation for sands. In: Proceedings of the second Pan American conference on soil mechanics and foundations engineering; 1963. p. 289–324.
[23] Chiu HC. Stable baseline correction of digital strong-motion data. Bull Seismol Soc Am 1997;87:932–44.
[24] Frankel AD, Carver DL, Williams RA. Nonlinear and linear site response and basin effects in Seattle for the M 6.8 Nisqually, Washington, earthquake. Bull Seismol Soc Am 2002;92:2090–109.
[25] Trifunac MD, Hao TY, Todorovska MI. On the reoccurrence of site specific response. Soil Dyn Earthq Eng 1999;18:569–92.
[26] Trifunac MD, Ivanović SS. Re-occurrence of site specific response in former Yugoslavia—Part I. Montenegro. Soil Dyn Earthq Eng 2003;23: 637–61.
[27] Trifunac MD, Ivanović SS. Re-occurrence of site specific response in former Yugoslavia—Part II: Friuli, Banja Luka and Kopaonik. Soil Dyn Earthq Eng 2003;23:663–81.
[28] Zeghal M, Elgamal AW, Tang HT, Stepp JC. Lotung downhole array. II: evaluation of soil nonlinear properties. J Geotech Eng 1995;121: 363–78.
[29] Chang CY, Mok CM, Tang HT. Inference of dynamic shear modulus from Lotung downhole data. J Geotech Eng 1996;122:657–65.
[30] Li XS, Shen CK, Wang ZL. Fully coupled inelastic site response analysis for 1986 Lotung earthquake. J Geotech Geoenviron Eng 1998;124: 560–73.
[31] Borja RI, Chao HY, Montáns FJ, Lin CH. Nonlinear ground response at Lotung LSST site. J Geotech Geoenviron Eng 1999;125:187–97.
[32] Borja RI, Lin CH, Sama KM, Masada GM. Modelling non-linear ground response of non-liquefiable soils. Earthq Eng Struct Dyn 2000;29:63–83.
[33] Huang HC, Shieh CS, Chiu HC. Linear and nonlinear behaviors of soft soil layers using Lotung downhole array in Taiwan. Terr Atoms Ocean Sci 2001;12:503–24.
[34] Hartzell S, Bonilla LF, Williams RA. Prediction of nonlinear soil effects. Bull Seismol Soc Am 2004;94:1609–29.
[35] Lee CT, Cheng CT, Liao CW, Tsai YB. Site classification of Taiwan free-field strong-motion stations. Bull Seismol Soc Am 2001;91:1283–97.